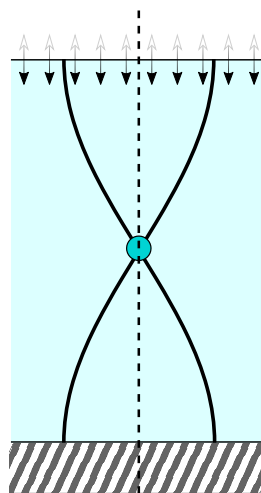


Bachelor Thesis

Acoustic levitation of particles

Andreas M. Munk
s135150



Supervisor: Professor Henrik Bruus

Department of Physics
Technical University of Denmark

23 June 2016

Abstract

Within the field of acoustofluidics, the topic of acoustic levitation describes how acoustic fields can be used to levitate particles by properly tuning the levitator device. Levitating conditions arise, when the acoustic radiation force exactly counteracts the force of gravity. Thus, a fundamental understanding of the radiation force is necessary in order to design acoustic levitators.

In this thesis, we study the acoustic radiation force in inviscid Newtonian fluids. We present the governing equations for such fluids, and use them to find standing waves at resonance, in an ideal levitator system with wavenumber $k_0 = 2\pi/\lambda$, with λ being the wavelength. We then derive an exact expression for the acoustic radiation force, originating from standing waves scattering off of spherical particles. The expression is written as an infinite sum, and is valid for any size particles, within the inviscid limit $a \gg \delta$, with δ being the viscous boundary layer width. This expression extends the current theory, which is a two term expression, a monopole and a dipole term, only valid for small particles, $\delta \ll a \ll \lambda$. Applying this expression on a levitator system consisting of a water droplet in air, we find that the acoustic radiation force deviates from a volumetric proportionality. We find, that the stable levitating positions shift towards the acoustic force's anti-nodes as the particle becomes larger relative to λ . Hence, a levitator eventually becomes unable to provide levitating condition, as the acoustic force lessens relative to the force of gravity for larger particles. Additionally, we find that including higher modes, than just the previous monopole and dipole modes, is necessary in order to account for the total force. As a final analytical result, we find that the acoustic radiation force oscillates with respect to the dimensionless wavenumber $x = k_0 a$, such that the force completely changes direction.

A final topic investigated in this thesis, is to determine the effect of using a concave reflector, and to find stable levitating positions in a more realistic levitator system. This is done by building an azimuthal symmetric model in Comsol. By running the simulations, we find that concave reflectors indeed improve the strength of the levitator, and that stable positions of levitation emerges.

These findings are interesting not only from a theoretical point of view, but also from an engineering perspective. The exact radiation force expression could be used to determine and adjust e.g. microgravitational condition for particles of radius $a \gtrsim \lambda$.

Preface

This thesis is submitted as a final project, as part of the Bachelor of Science degree in Earth and Space Physics and Engineering, at the Technical University of Denmark (DTU). The thesis was written at the Department of Physics in the Theoretical Microfluidics Group (TMF) headed by Professor Henrik Bruus over the course of five months equivalent to 15 ETCS points.

Above all, I would like to thank my supervisor Professor Henrik Bruus for his outstanding guidance and dedication towards his students, and last but not least I would like to thank him for sharing his immense physical knowledge in inspiring and motivational ways. Being part of TMF has been a great educational journey, and I would like to thank the entire group for being welcoming, eager to share information with each other, and of course for hosting great social events.

Special thanks goes to PhD student, Jonas Karlsen, for spending hours on end, discussing various physical topics. It has been a key factor for my understanding of microfluidics. I would also like to thank PhD student, Mikkel Ley, for assisting me whenever I encountered issues in Comsol. The two of them have made me feel part of TMF. Thanks to my fellow BSc student, Jakob Hauge, with whom I have been introduced to acoustofluidics and developed an understanding for this topic.

Finally, I would like to thank my parents for being encouraging and supportive and always believing in my endeavors.

Andreas M. Munk
Department of Physics
Technical University of Denmark
23 June 2016

Contents

List of figures	ix
List of tables	xi
List of symbols	xiii
1 Introduction	1
1.1 The levitator	2
1.2 Outline of this thesis	4
2 Basic acoustic theory	7
2.1 Defining scalar- and vector fields	7
2.2 The continuity equation	8
2.3 Navier–Stokes equation	8
3 Weak form modeling in Comsol	11
3.1 The finite element method	11
4 First-order solutions to inviscid fluids	13
4.1 First-order perturbation theory	13
4.1.1 The general representation of the velocity field and thermoviscous and viscous boundary layers	15
4.2 Ideal levitator solutions	16
4.3 Physical parameters	19
4.3.1 Final notes on the Quality factor	19
5 Acoustic radiation force exerted on small particles	21
5.1 Second-order perturbation theory	21
5.2 The acoustic radiation force	22
5.3 The general wave expansion	24
6 Acoustic radiation force exerted on large particles	29
6.1 Exact acoustic radiation force from a standing wave	29
6.2 Resultant forces from an acoustic standing wave	35
6.3 Levitating a particle	38

6.4	Range of validity	42
6.4.1	Time oscillation	42
6.4.2	Boyancy force	43
6.4.3	Small particle oscillations	43
7	Simulating a single-axis levitator	45
7.1	Setting up Comsol	46
7.2	Results	47
8	Conclusion and outlook	51
A	Appendix to Chapter 3	53
A.1	Implementing PML	53
B	Appendix to Chapter 4	55
B.1	The general representation of the velocity field and thermoviscous and vis- cous boundary layers	55
B.2	Complete treatment of the solution to the ideal levitator setup	56
B.3	Ignoring non-resonant component	57
B.4	Acoustic energy density for harmonic waves	59
C	Appendix to Chapter 5	61
C.1	Special functions	61
C.2	Deriving Eq. (5.19)	62
D	Appendix to Chapter 6	63
D.1	Integration of tripple Legendre and Gegenbauer polynomials	63
D.2	Derivation of Eq. (6.20)	65
E	Appendix to Chapter 7	67
E.1	Solving Helmholtz wave equation in cylindrical coordiantes	67
E.2	Parameters used in Comsol	68
	Bibliography	70

List of Figures

1.1	Realistic levitator	3
3.1	Mesh and associated testfunctions in Comsol.	12
4.1	Ideal levitator wave generator	16
5.1	Ratio of the scattering coefficients, A_n	27
6.1	A levitating particle	30
6.2	Comparison between $F_{\text{exact}}^{\text{rad}}$ and $F_{\text{sa}}^{\text{rad}}$	36
6.3	Direction of the radiation force	38
6.4	Stable position of levitation	39
6.5	Spatial oscillating radiation force	40
6.6	Interpretations of the ideal levitator models for larger x	41
7.1	Model of the levitator geometry in Comsol.	46
7.2	Frequency response of the single-axis levitator.	47
7.3	Acoustic fields actuated in the single axis levitator.	48
7.4	Absolute value of the velocity field in Comsol	49
7.5	Stability of the levitator	50
A.1	Manually implemented PML	54

List of Tables

4.1	Physical parameters	19
4.2	Calculated parameters	19

List of symbols

Symbol	Description	Unit
ρ	Mass density	kg m^{-3}
p	Pressure	N m^{-2}
ϕ	Velocity scalar potential	$\text{m}^2 \text{s}^{-1}$
\mathbf{v}	Velocity vector	m s^{-1}
$\boldsymbol{\sigma}$	Cauchy stress tensor	N m^{-2}
\mathbf{f}	Body force density	N m^{-3}
\mathbf{g}	Acceleration of gravity	N kg^{-1}
ϕ	Velocity scalar potential	$\text{m}^2 \text{s}^{-1}$
$(\bullet)_0, (\bullet)_1, (\bullet)_2$	zeroth-, first- and second-order of \bullet	
η_0	Dynamic viscosity	$\text{kg m}^{-1} \text{s}^{-1} = \text{Pa s}$
η^b	Bulk viscosity	$\text{kg m}^{-1} \text{s}^{-1} = \text{Pa s}$
$\nu_0 = \eta_0 / \rho_0$	Momentum diffusion constant	$\text{m}^2 \text{s}^{-1}$
$\beta = \eta^b / \eta_0 + 1/3$	Viscosity ratio	1
c_0	Isentropic speed of sound	m s^{-1}
κ_0	Isentropic compressibility	Pa^{-1}
t	Time	s
f	Frequency	Hz
$\omega = 2\pi f$	Angular frequency	s^{-1}
λ	Wavelength	m
$\delta = \sqrt{2\nu_0/\omega}$	Viscous boundary width	m
δ_t	Thermoviscous boundary width	m
k_0	Undamped wave number	m^{-1}
$\Gamma = \frac{(1+\beta)\omega\eta_0}{2\rho_0 c_0^2}$	Viscous dampening factor	1
ϑ_n	P. 30 coefficient	1
v_{bc}	Actuation velocity amplitude	m s^{-1}
L	Levigator length	m
R	Radius of simulated levitator	m
Q	Quality factor of resonance	1
E_{ac}	Time-averaged acoustic energy density	J/m^3

Symbol	Description	Unit
a	Particle radius	m
$\mathbf{F}_{sa}^{\text{rad}}$	Small argument acoustic radiation force	N
$\mathbf{F}_{\text{exact}}^{\text{rad}}$	Exact acoustic radiation force	N
$(\bullet)_p$	Particle parameter \bullet	
$x = k_0 a$		1
∂_j	Partial derivative with respect to j	$[j]^{-1}$
∇	Gradient operator	m^{-1}
$\nabla \cdot$	Divergence operator	m^{-1}
$\nabla \times$	Rotation operator	m^{-1}
∇^2	Laplacian	m^{-2}
(x, y, z)	Cartesian coordinates	m
(r, θ, z)	Cylindrical coordinates	
(r, θ, φ)	Spherical coordinates	
\mathbf{e}_j	Unit vector in the j th direction	
\mathbf{n}	Surface normal vector	
$\langle \bullet \rangle$	Time-average of \bullet	
$ \bullet $	Absolute value of \bullet	
$(\bullet)^*$	Complex conjugate of \bullet	
$\text{Re}[\bullet]$	Real part of \bullet	
$\text{Im}[\bullet]$	Imaginary part of \bullet	
$i^2 = -1$	Imaginary unit	
e	Base of the natural logarithm	
P_n	Legendre polynomial of order n	
J_n	Bessel function (1st) of order n	
j_n	Spherical Bessel function (1st) of order n	
h_n	Spherical Hankel function (1st) of order n	

Chapter 1

Introduction

Acoustic levitation is a phenomenon in which ultrasound waves are used to lift and hold small particles suspended in a fluid, due to the so-called acoustic radiation force. This force, responsible for the levitation, is a consequence of acoustic wave scattering. The research field of acoustofluidics is a combination of the fields of microfluidics and acoustics. In the past few decades, there has been an increased interest in acoustofluidics, due to its many applications, such as acoustic levitator systems, and especially in relation to lab-on-a-chip devices. Twenty-three articles, reviewing the fundamental theory and various experiments of lab-on-a-chip devices, have been published in the journal “Lab on a chip” [1], as an extensive tutorial. Important examples of lab-on-a-chip applications are detection of cancer cells in blood [2] and separation of lipids from blood [3]. Such experiments are commonly known as acoustophoresis, and it may prove to revolutionize medical- analysis and diagnostics.

To optimize modern acoustofluidic devices, a fundamental understanding of the acoustic radiation force is therefore necessary. The theoretical development began in 1934 when Louis V. King [4] studied the radiation force exerted on a small spherical incompressible solid with radius a , much smaller than the applied acoustic wavelength λ , i.e. $a \ll \lambda$, in an inviscid fluid. Later, in 1955, the theory was extended by Yosioka and Kawasima [5], to include a small elastic solid, and by that also fluid droplets, though still in an inviscid fluid. A simpler method of calculating the radiation force on small elastic solids or droplets in inviscid fluids, was developed in 1962 by Gorkov [6], in order to summarize the work done by Yosioka, Kawasima and King.

At that time of the early studies, the viscous effects were completely neglected. However, viscous effects become relevant when the elastic solid or droplet size reaches a lower limit, $a \lesssim \delta$, where δ is the acoustic boundary layer, which depends on the viscosity. Thus when $\delta \sim a \ll \lambda$, the viscous effect can no longer be ignored. Analytical studies of the radiation force in the limit $a \ll \delta \ll \lambda$ and $\delta \ll a \ll \lambda$ was first done by Doinikov [7–9], who included thermoviscous and viscous effects, thereby introducing the thermal boundary layer, δ_t . However, further analysis was still needed in the limit $a \sim \delta$, which was subsequently performed by Settnes and Bruus in 2011 [10]. They developed a general theoretical expression for the radiation force for an arbitrary viscous boundary

layer width, in the adiabatic limit, but ignored the thermal boundary layers i.e. thermoviscous effects. In 2015, Karlsen and Bruus [11] developed a final theory explaining the radiation force, including thermoviscous and viscous effects in the small elastic solid or droplet limit, $\delta_t, \delta, a \ll \lambda$, with no further restriction between δ_t, δ and a . Karlsen and Bruus conclude that $\delta_t \sim \delta$ and that if $\delta_t, \delta \ll a$, the viscous and thermoviscous effects can be completely neglected. The final derived analytical expression for the radiation force is a monopole term and a dipole term of an otherwise infinite sum, due to higher modes being neglectable [12]. The two terms are related to the expansion and compression of the suspended particle (monopole) as well as the back-and-forth oscillation (dipole).

One aspect however, that none of the above-mentioned scientist have touched upon, is the steady-state deformation of a spherical elastic solid or droplet experiencing acoustic forces. In the steady-state shape, the elastic solid or droplet loses its spherical symmetry, and consequently alters the integration of stresses exerted on the surface of the suspended elastic solid or droplet. This leads to a different radiation force. The effects of the steady-state shape have been studied in an extensive article written by Yarin, Pfaffenlehner and Tropea [13], which the reader is encouraged to read, as we in this thesis will ignore the permanent deformation and assume spherical steady-shape.

Other important research within the field of acoustic radiation force exerted on non-spherical particles, is done by Wijaya and Lim [14]. They created a three-dimensional boundary element model and analyzed non-spherical particles subjected to acoustic Bessel beams.

1.1 The levitator

In this thesis, we will focus on actuated standing waves in the levitator setup, also known as the single-axis levitator, in which an elastic solid or droplet is suspended. The purpose of the levitator is to balance the force of gravity with an opposite directed acoustic radiation force, and find stable levitational conditions.

In the case of a small droplet or elastic solid where $\delta, \delta_t \ll a \ll \lambda$ the acoustic radiation force is proportional to the volume of the droplet or elastic solid, as shown by Settnes and Bruus. Consequently, as the force of gravity is likewise proportional with said volume, the balancing of the two forces is independent of the droplet or elastic solid size, and the levitation position depends only on the amplitude of the acoustic fields. However, when $a \sim \lambda$ this can no longer be assumed to be true. Since the levitator is not limited to small droplets or small elastic solids, it is the primary goal of this thesis to examine the importance of the size of the droplet or elastic solid, when balancing the acoustic radiation force and the gravitational force.

An ideal single-axis levitator is illustrated on the frontpage. The name refers to the actuation in one direction and the accompanying azimuthal symmetry around the coaxial of the vibrating device and reflector, usually aligning with the direction of gravity.

In reality, the standing acoustic wave is not perfect, as the wave is actuated by a finite vibrating device - see Fig. 1.1. Thus, outside the volume enclosed by the actuator and reflector, the acoustic wave will propagate outwards and dissipate or experience undesired

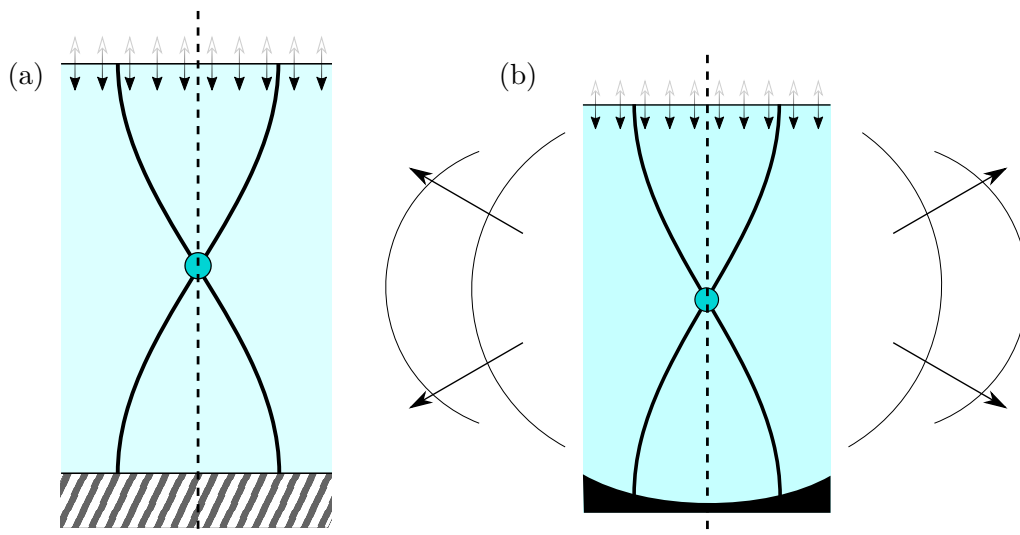


Figure 1.1: (a) Frontpage figure. (b) The setup of a simple more realistic levitator. The center dotted line represents the azimuthal symmetric coaxis. Notice the concave bottom reflector which focuses the reflective waves towards the centerline, thus creating an approximated standing wave in which a elastic solid or droplet (cyan) is suspended. The waves propagating away from the levitator are due to the finite setup.

reflections, which could create small disruptions on the waveform between the actuator and reflector. However, by properly designing the reflector, which is usually concave, a standing wave can be assumed along the coaxis normal to the actuator. The wave will thus deviate from the standing acoustic wave form as a function of distance to the axis of symmetry. The stability and levitation capabilities of a real levitator can be greatly improved by tuning the reflector. The effects and improvements due to reflector design has been analyzed and experimented on by Xie and Wei [15]. They achieved stable levitation of high-density materials such as tungsten.

Acoustic levitation has several application such as creating microgravitational environments and for material processing, where material contamination from container walls can be avoided, as discussed by Brandt [16]. The microgravity conditions are further highly useful to scientist, as otherwise space bound experiments can be performed on earth. Acoustic levitation has also been concluded superior to magnetic or electric levitation for microassembly purposes, as acoustic levitation is not limited by conducting or magnetic properties of materials [17].

Due to the single-axis levitator's many applications and benefits, the special case of acoustofluidics called acoustic levitation deserves to be analysed specifically. This thesis will therefore derive an exact expression for the acoustic radiation force for spherical arbitrary size elastic solids or droplets in the limit $\delta, \delta_t \ll a, \lambda$ with no further restrictions. This limit allows us to ignore thermoviscous and viscous effects. The analytically analysed levitator system will be assumed to be ideal, i.e. the actuator and reflector are assumed

to be infinitely wide, prohibiting any wave dissipation. Additionally, we will assume the wave propagation to be isentropic, and so all processes in the system are adiabatic. This approximation is based on the assumption that the expansion and compression of the fluid is on a time scale much smaller, than that of the energy-exchange with the surroundings. The motivation for deriving such an expression is to account for higher modes than the monopole and dipole modes, and analyse the development of the exact radiation force as function of the ratio between a and λ , to see how higher modes may become relevant in the $a \gtrsim \lambda$ limit. We will subsequently balance the radiation force with the force of gravity in a system, where we suspend a water droplet in air. This allows us to address the main issue in this thesis: to determine stable microgravitaional conditions, i.e. stable positions of levitation, as a function of radius and wavelength ratio.

Finally, the numerical solver, Comsol, will be used to simulate a single-axis levitator system, where the actuator and reflector have finite width. Again we assume we suspend a water droplet in air. The purpose is to qualitatively assess the effect of implementing a concave reflector, and to evaluate how well standing waves will be actuated. We will subsequently calculate the small particle limit radiation force found by Settnes and Bruus, and determine the stability of the levitator.

1.2 Outline of this thesis

Chapter 2: Basic acoustic theory

A definition of the scalar- and vector fields as well as the two governing equations, relevant to this thesis, are presented.

Chapter 3: Weak form modeling in Comsol

A brief walkthrough of how the finite element method is applied in Comsol, and how to formulate the weak form partial differential equations used in Comsol.

Chapter 4: First-order solutions to inviscid fluids

This chapter explains how first-order perturbations theory is applied in acoustofluidics, and how we define inviscid fluids. We will argue for, why we in this thesis can assume inviscid fluids, and we will solve the Helmholtz wave equation for an ideal levitator and discuss the solution.

Chapter 5: Acoustic radiation force exerted on small particles

This chapter explains how second-order perturbations theory is applied, and how this results in an acoustic radiation force. Thereafter, the result found by Settnes and Bruus will be presented. Subsequently, the general wave expansion in spherical coordinates of the acoustic fields will be introduced, in order to begin the treatment of the acoustic radiation force in the acoustic force in the limit $a \gtrsim \lambda$.

Chapter 6: Acoustic radiation force exerted on large particles

Using the results from the previous chapter, the exact analytical expression for the acoustic radiation force is derived for a standing wave. This expression is compared with the expression of the radiation force in the small particle limit, found by the Settnes and Bruus. We then investigate how the stable position of levitation varies as function of the dimensionless wavenumber $x = k_0 a$, in order to determine the behavior of stable levitation.

Chapter 7: Simulating a single-axis levitator

This chapter presents and discuss the results from a single-axis levitator simulation constructed in Comsol. The purpose of this chapter is to analyze the effect of a concave reflector, as well as qualitatively analyse the actuated acoustic fields pursue of standing waves. The stability of the simulated levitator will be discussed. Finally, possible stable levitation is assesed.

Chapter 8: Conclusion and outlook

Analytical and graphical results will be summarised and presented, and future analytical and numerical work is suggested.

Appendix: A, B, C, D and E

More detailed elaboration on various important subjects. Relevant derivations and calculations used in obtaining the results in the main chapters, are found in these appendices.

Chapter 2

Basic acoustic theory

To investigate the acoustic effect on a particle suspended in a fluid, we will in this chapter present the governing equations for a viscous and compressible Newtonian fluid, namely the continuity equation and Navier–Stokes equation. This chapter is written by following the work of Henrik Bruus [18].

2.1 Defining scalar- and vector fields

We will first off introduce the primary scalar field and vector fields described as continuum fields. As we will be investigating acoustic effect on fluids, we will operate in the Eulerian frame, i.e. the investigated fields will be described around a stationary point \mathbf{r} . Consequently, position \mathbf{r} and time t are independent variables.

By using the continuum description, any field will be defined by a fixed time-averaged subvolume, \mathcal{V} , containing a dynamically changing amount of molecules

$$F(\mathbf{r}, t) = \langle F(\mathbf{r}', t) \rangle_{\mathbf{r}' \in \mathcal{V}}. \quad (2.1)$$

We thus define the density scalar field ρ , and velocity vector field \mathbf{v} as

$$\rho(\mathbf{r}, t) = \frac{1}{\mathcal{V}} \sum_{i \in \mathcal{V}} m_i, \quad \mathbf{v}(\mathbf{r}, t) = \frac{1}{\rho(\mathbf{r}, t)\mathcal{V}} \sum_{i \in \mathcal{V}} m_i \mathbf{v}_i, \quad (2.2)$$

where m_i and v_i refers to the mass and velocity respectively of particle i within the subvolume.

The continuum description is valid down to a few nm [19]. However, this limit depends on the size of the molecules.

As a final note to this section, we will for future use, list the gradient, divergence and Laplacian

$$\nabla f(x, y, z), \quad \text{the gradient of a scalarfield,} \quad (2.3a)$$

$$\nabla \cdot \mathbf{a}(x, y, z), \quad \text{the divergence of vectorfield } \mathbf{a}, \quad (2.3b)$$

$$\nabla \cdot \nabla \mathbf{v} = \nabla^2 \mathbf{v} = \nabla (\nabla \cdot \mathbf{v}) - \nabla \times \nabla \times \mathbf{v}, \quad \text{the Laplacian on vector } \mathbf{v}. \quad (2.3c)$$

2.2 The continuity equation

The continuity equation is an expression of conservation of mass. The mass $M(\mathcal{V}, t)$ within a subvolume \mathcal{V} can be written as;

$$M(\mathcal{V}, t) = \int_{\mathcal{V}} d\mathbf{r} \rho(\mathbf{r}, t). \quad (2.4)$$

The change in mass in time must be due to mass flux through the surface $\partial\mathcal{V}$ of the subvolume \mathcal{V} . This inward flux can be expressed as mass density times an advective velocity, and using that any investigated subvolume, \mathcal{V} , is fixed in time as of Section 2.1, we find

$$\partial_t M(\mathcal{V}, t) = \int_{\mathcal{V}} d\mathbf{r} \partial_t \rho(\mathbf{r}, t) = - \oint_{\partial\mathcal{V}} da \rho(\mathbf{r}, t) \mathbf{v}(\mathbf{r}, t) \cdot \mathbf{n}. \quad (2.5)$$

With use of Gauss theorem we obtain,

$$\int_{\mathcal{V}} d\mathbf{r} \partial_t \rho(\mathbf{r}, t) = - \int_{\mathcal{V}} d\mathbf{r} \nabla \cdot (\rho(\mathbf{r}, t) \mathbf{v}(\mathbf{r}, t)). \quad (2.6)$$

This holds true for all subvolumes \mathcal{V} , and thus we arrive at,

$$\partial_t \rho(\mathbf{r}, t) = - \nabla \cdot [\rho(\mathbf{r}, t) \mathbf{v}(\mathbf{r}, t)], \quad (2.7a)$$

$$\partial_t \rho(\mathbf{r}, t) = - \partial_j [\rho(\mathbf{r}, t) v_j(\mathbf{r}, t)], \quad \text{in index notation.} \quad (2.7b)$$

2.3 Navier–Stokes equation

The Navier–Stokes equation governs the change of momentum $\partial_t P_i$ within a subvolume \mathcal{V} . The equation accounts for changes of momentum due to body forces, advection, viscous friction and pressure normal to the volume, respectively labeled P^{body} , P^{adv} , P^{visc} and P^{press} . For simplicity, the position and time dependencies are implicit, whenever we write ρ , p or \mathbf{v} , unless otherwise specified. The total change of momentum is then expressed in terms of the fluid density ρ , the pressure $p(\rho)$, velocity field \mathbf{v} and the stress tensor of the fluid $\boldsymbol{\sigma}$ as,

$$\partial_t P_i = \partial_t \int_{\mathcal{V}} d\mathbf{r} \rho(\mathbf{r}, t) v_i(\mathbf{r}, t) = \int_{\mathcal{V}} d\mathbf{r} f_i - \oint_{\partial\mathcal{V}} da \{n_j \rho v_j v_i - n_j \sigma_{ij}\}. \quad (2.8)$$

Assuming a Newtonian fluid, the stress tensor is written in terms of ρ , p , \mathbf{v} , dynamic shear viscosity η_0 , bulk viscosity η^b , and viscous ratio $\beta = (\eta^b/\eta_0 + \frac{1}{3})$ [20],

$$\sigma_{ij} = -p \delta_{ij} + \eta_0 (\partial_j v_i + \partial_i v_j) + (\beta - 1) \eta_0 (\partial_k v_k \delta_{ij}), \quad \text{and} \quad f_i = (\rho \mathbf{g})_i. \quad (2.9)$$

Using vector notation, the stress tensor is written as,

$$\boldsymbol{\sigma} = -p \mathbf{I} + \eta_0 (\nabla \mathbf{v} + (\nabla \mathbf{v})^T) + (\beta - 1) \eta_0 (\nabla \cdot \mathbf{v}) \mathbf{I}, \quad (2.10)$$

where \mathbf{I} is the identity matrix and superscript ‘‘T’’ denotes the usual matrix transposition.

Using Gauss theorem, Eq. (2.7) and noting this has to hold for every subvolume \mathcal{V} , one finds the Navier–Stokes equation written as,

$$\rho \partial_t v_i + \rho v_j \partial_j v_i = \rho g_i - \partial_j \sigma_{ij} - \partial_i p. \quad (2.11)$$

For a Newtonian fluid at a fixed temperature, the shear- and bulk viscosities, η_0 and η^b can be considered constant and Eq. (2.11) reduces to,

$$\rho \{ \partial_t v_i + v_j \partial_j v_i \} = \rho g_i - \partial_i p + \eta_0 \partial_j^2 v_i + \beta \eta_0 \partial_i (\partial_j v_j), \quad (2.12a)$$

and written by using common vector notation,

$$\rho \{ \partial_t \mathbf{v} + (\mathbf{v} \cdot \nabla) \mathbf{v} \} = \rho \mathbf{g} - \nabla p + \eta_0 \nabla^2 \mathbf{v} + \beta \eta_0 \nabla (\nabla \cdot \mathbf{v}). \quad (2.12b)$$

Throughout this thesis, we will ignore the external force of gravity when operating with Navier–Stokes equation, as the applied acoustic pressure fields are typically of order $p_{\text{applied}} \sim 10^3$ Pa. Compared to the difference of hydrostatic pressure inside levitators, where the distance h , between acutator and reflector is of order a few centimeters, we calculate the hydrostatic pressure to be of order $\Delta p_{\text{hydro}} = \rho_0 g h \sim 1$ Pa (assuming that the fluid is air). Hence $\Delta p_{\text{hydro}} \ll p_{\text{applied}}$. Thus, Eq. (2.12) reduces to,

$$\rho \{ \partial_t \mathbf{v} + (\mathbf{v} \cdot \nabla) \mathbf{v} \} = -\nabla p + \eta_0 \nabla^2 \mathbf{v} + \beta \eta_0 \nabla (\nabla \cdot \mathbf{v}), \quad (2.13a)$$

$$\rho \{ \partial_t \mathbf{v} + (\mathbf{v} \cdot \nabla) \mathbf{v} \} = -\nabla p, \quad \text{for an inviscid fluid.} \quad (2.13b)$$

Chapter 3

Weak form modeling in Comsol

This chapter serves to be a brief introduction to manually determine and apply the weak form partial differential equations (PDE). Additionally, a method of applying appropriate boundary conditions will be shown. This chapter is written by following Christoffer Nielsen [21] and Henrik Bruus [22].

3.1 The finite element method

In general, most governing equations in field theory has the following form

$$\nabla \cdot \mathbf{J} - F = 0, \quad (3.1)$$

where $\mathbf{J}(g(\mathbf{r}))$ is a flux of field variable $g(\mathbf{r})$ and F is a force driving the flux. The exact solution to Eq. (3.1) is called a strong solution. However, the finite element method solves problems in the form of Eq. (3.1), by constructing a mesh domain representing a real physical domain and associating a localized basis function $\hat{g}_m(\mathbf{r})$ (called “testfunctions” in Comsol) on each mesh node. These localized basis function are constructed in such a way that they evaluate to 1 on their associated node, and vary in some way to 0 on all neighbouring nodes. This is illustrated in Fig. 3.1. Additionally, these functions nearly span the entire function space, thus we can write the $g(\mathbf{r})$ as a superposition of $\hat{g}_n(\mathbf{r})$,

$$g(\mathbf{r}) = \sum_n c_n \hat{g}_n(\mathbf{r}). \quad (3.2)$$

Using this expansion, a defect d is introduced and we rewrite Eq. (3.1)

$$\nabla \cdot \mathbf{J}(\sum_n c_n \hat{g}_n(\mathbf{r})) - F = d(\mathbf{r}). \quad (3.3)$$

The strong solution is the case where $d(\mathbf{r}) = 0$. However, in Comsol an approximate solution to Eq. (3.1) is found by forcing the defect to vanish, when projected onto each node of the mesh, i.e. a volume integral

$$\langle \hat{g}_m(\mathbf{r}), d \rangle \equiv \int_{\Omega} [\hat{g}_m(\mathbf{r}) d(\mathbf{r})] dV = 0, \quad \forall m. \quad (3.4)$$

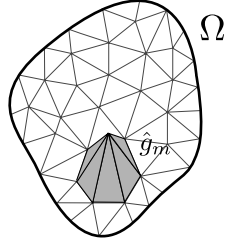


Figure 3.1: Illustration of testfunction $\hat{g}_m(\mathbf{r})$ in a two-dimensional space Ω . Note how in this case the test function is linear.

Inserting Eq. (3.3) into Eq. (3.4), we find

$$\langle \hat{g}_m(\mathbf{r}), d \rangle = \langle \hat{g}_m(\mathbf{r}), \nabla \cdot \mathbf{J}(g(\mathbf{r})) \rangle - \langle \hat{g}_m(\mathbf{r}), F \rangle = 0, \quad \forall m. \quad (3.5)$$

Due to the linearity of ∇ , one arrives at a matrix problem,

$$\mathbf{K} \mathbf{c} = \mathbf{f}, \quad (3.6)$$

where $\mathbf{f}_m = \langle \hat{g}_m(\mathbf{r}), F \rangle$ and $K_{mn} = \langle \hat{g}_m(\mathbf{r}), \nabla \cdot \mathbf{J}(\hat{g}_n(\mathbf{r})) \rangle$. Comsol solves Eq. (3.6) by determining the expansion coefficients c_n and to do so we need a way of specifying appropriate boundary conditions for a given physical problem. To do this we can apply Gauss theorem on Eq. (3.5), and note that $\nabla \cdot (\hat{g}_m(\mathbf{r}) \mathbf{J}) = \hat{g}_m(\mathbf{r}) \nabla \cdot \mathbf{J} + \nabla \hat{g}_m(\mathbf{r}) \cdot \mathbf{J}$, to arrive at

$$\int_{\partial\Omega} [\hat{g}_m(\mathbf{r}) \mathbf{J} \cdot \mathbf{n}] ds + \int_{\Omega} [-\nabla \hat{g}_m(\mathbf{r}) \cdot \mathbf{J} - \hat{g}_m(\mathbf{r}) F] dV = 0. \quad (3.7)$$

Hence, we find a surface integral to which one can apply boundary conditions, as well as a volume integral.

A Neumann boundary condition $N(\mathbf{r})$, is easily imposed by letting $\mathbf{J} \cdot \mathbf{n} = N(\mathbf{r})$ in the surface integral. In general, one can impose a boundary condition $R(\mathbf{r})$ by introducing a Lagrange multiplier, $\lambda(\mathbf{r})$ with the associated testfunction $\hat{\lambda}_m(\mathbf{r})$ on the boundary. With this we can write,

$$\int_{\partial\Omega} [\hat{g}_m(\mathbf{r}) \lambda(\mathbf{r}) + \hat{\lambda}_m(\mathbf{r}) R(\mathbf{r})] ds + \int_{\Omega} [-\nabla \hat{g}_m(\mathbf{r}) \cdot \mathbf{J} - \hat{g}_m(\mathbf{r}) F] dV = 0, \quad (3.8)$$

where $\int_{\partial\Omega} \hat{\lambda}_m(\mathbf{r}) R(\mathbf{r}) ds = 0$, since $\hat{\lambda}_m(\mathbf{r})$ is completely independent of $\hat{g}_m(\mathbf{r})$. A common boundary condition is Dirichlet, where $R(\mathbf{r}) = g(\mathbf{r}) - D(\mathbf{r})$.

It should be noted that the above method is not restricted to only scalar forces F . In the case where the flux-driving force is a vector, \mathbf{F} , and hence the flux is a tensor, the above-mentioned treatment should be made for each component of \mathbf{F} . This requires three different kinds of testfunctions.

Finally, when solving acoustical problems in Comsol, where one is dealing with acoustic waves propagating in various direction, it is often desirable to have domains, which simulates infinite propagation in any arbitrary direction. These domains are named ‘‘Perfectly matched layers’’ (PML). A mathematical formulation is found in Appendix A.1. In Chapter 7 we will simulate a single-axis levitator using preprogrammed modules and PML in Comsol.

Chapter 4

First-order solutions to inviscid fluids

The continuity and Navier–Stokes equations, Eqs. (2.7) and (2.13), together with the equation of state $p(\rho)$, form a set of coupled non-linear partial differential equations. Considering the difficulty of solving this analytically, a good approximated solution can be achieved through perturbation theory.

In this chapter we will find the resulting first-order continuity and Navier–Stokes equations, and subsequently find the acoustic wave solution to the ideal levitator system. The earlier-mentioned acoustic radiation force is evidently a result of second-order perturbation theory, and will be treated in the next chapter.

We will in general assume the following, when taking any fluid into consideration; the unperturbed system is assumed homogeneous with constant density ρ_0 , constant pressure p_0 and zero velocity field, i.e. $\mathbf{v}_0 = \mathbf{0}$. The derivation and analysis of first-order perturbation theory, can be read in Ref. [12] This chapter’s first section merely summarizes it.

4.1 First-order perturbation theory

When applying weak acoustic fields to a fluid, the system experiences tiny perturbations, and we can thus write the fields of density, pressure and velocity as,

$$p = p_0 + p_1 = p_0 + c_0^2 \rho_1, \quad \rho = \rho_0 + \rho_1, \quad \mathbf{v} = \mathbf{0} + \mathbf{v}_1, \quad (4.1)$$

where we used that for an isentropic system, the Taylor expansion of $p(\rho)$ in $\rho = \rho_0 + \rho_1$ at ρ_0 , becomes $p(\rho) = p_0 + \left(\partial p / \partial \rho \Big|_{\rho=\rho_0}\right)_s \rho_1$, with superscript “s” denoting isentropic expansion. c_0 is here introduced as the isentropic speed of sound, as the derivative has dimensions velocity squared. c_0 is indeed the velocity of sound squared as concluded in Ref. [18]. For completeness we will for future use, introduce the adiabatic compressibility,

$$\kappa_0 = -\frac{1}{V} \left(\frac{\partial V}{\partial p}\right)_s = \frac{1}{\rho_0} \left(\frac{\partial \rho}{\partial p}\right)_s = \frac{1}{\rho_0 c_0^2}. \quad (4.2)$$

When substituting Eq. (4.1) into Eqs. (2.7) and (2.13), and neglecting terms higher than first order, we arrive at the following Navier–Stokes and continuity equations,

$$\partial_t \rho_1 = -\rho_0 \nabla \cdot \mathbf{v}_1, \quad (4.3a)$$

$$\rho_0 \partial_t \mathbf{v}_1 = -c_0^2 \nabla \rho_1 + \eta_0 \nabla^2 \mathbf{v}_1 + \beta \eta_0 \nabla (\nabla \cdot \mathbf{v}_1). \quad (4.3b)$$

By taking the time derivative of Eq. (4.3a), inserting this into the divergence of Eq. (4.3b) we arrive at,

$$\partial_t^2 \rho_1 = c_0^2 \left\{ 1 + \frac{(1 + \beta) \eta_0}{\rho_0 c_0^2} \partial_t \right\} \nabla^2 \rho_1. \quad (4.4)$$

We can without loss of generality, due to the linearization of the Navier–Stokes equations, Eq. (4.3b), assume time harmonic dependencies of all fields, as any time dependent field can be expressed by a fourier expansion of time harmonic fields by virtue of the fourier transform. The mathematical treatment of an aperiodic time dependent field is different than that of a periodic time dependent field. The periodic field can be expressed as a sum of harmonic fields, whereas the aperiodic field can be expressed as an integral over harmonic fields.

Thus, having solved for one frequency, one can find solutions for all frequencies. A second argument for looking at the time harmonic fields, is that in practice, actuated fields in acoustofluidics, are most commonly time harmonic.

The three acoustic fields are therefore assumed to be expressed as,

$$\rho_1(\mathbf{r}, t) = \rho_1(\mathbf{r}) e^{-i\omega t}, \quad p_1(\mathbf{r}, t) = p_1(\mathbf{r}) e^{-i\omega t}, \quad \mathbf{v}_1(\mathbf{r}, t) = \mathbf{v}_1(\mathbf{r}) e^{-i\omega t}, \quad (4.5)$$

where $\omega = 2\pi f$ is the angular frequency and f is the frequency. The complex time dependency is used, as it is the most general representation and mathematically simple to operate with. The real physical fields are the real part of Eq. (4.5).

By virtue of the harmonic time dependencies, we can simply substitute $\partial_t \rightarrow -i\omega$ everywhere in Eq. (4.4), letting us write,

$$\nabla^2 \rho_1 = -k^2 \rho_1, \quad (4.6a)$$

$$k = \frac{\omega}{c_0} \left(1 - i\omega \frac{(1 + \beta) \eta_0}{\rho_0 c_0^2} \right)^{-1/2} \approx k_0 (1 + i\Gamma), \quad \text{with } \Gamma = \frac{(1 + \beta) \omega \eta_0}{2\rho_0 c_0^2}, \quad (4.6b)$$

where we introduced the wavenumber $k_0 = \omega/c_0$, the viscous dampening factor Γ , and performed a Taylor expansion of k in 2Γ around $\Gamma_0 = 0$, assuming $\Gamma \ll 1$. Referring to Table 4.2, we find for air $\Gamma_{\text{air}} \simeq 3 \times 10^{-5}$, and Γ_{air} is indeed much smaller than one.

Eq. (4.6) is the Helmholtz wave equation, and as $\Gamma \ll 1$, we can in “bulk” neglect the viscosity effect completely, i.e. $k = k_0$. Thus, letting us rewrite Eq. (4.3b) by inserting Eq. (4.3a),

$$\mathbf{v}_1 = -i \frac{\nabla p_1}{\rho_0 \omega} = \nabla \phi_1, \quad \text{for } \eta_0 = 0, \quad (4.7)$$

implying that \mathbf{v}_1 is the gradient of the velocity potential $\phi_1 = -i\frac{p_1}{\rho_0\omega}$, where $[\phi_1] = \text{m}^2 \text{s}^{-1}$. Eq. (4.7) further show that, since $\phi_1 \propto p_1 \propto \rho_1$ and that the operators ∂_t and ∇ commutes, the Helmholtz wave equation Eq. (4.6) holds true for both ϕ_1 , p_1 and \mathbf{v}_1 as well as ρ_1 .

Another special case worth investigating is the case where Eq. (2.3c) reduces to $\nabla^2 \mathbf{v}_1 = \nabla(\nabla \cdot \mathbf{v}_1)$, e.g. when $\nabla \times \mathbf{v}_1 = \mathbf{0}$. Thus, we can express Eq. (4.3b), by inserting Eq. (4.3a), and performing some rewriting (much similar to that made for Eq. (4.6)), as

$$\mathbf{v}_1 = -\frac{i}{\omega\rho_0(1+i\Gamma)^2} \nabla p_1 = \nabla \phi_1, \quad \text{with} \quad \nabla^2 \mathbf{v}_1 = \nabla(\nabla \cdot \mathbf{v}_1), \quad \text{and} \quad \Gamma = \frac{\eta_0\omega(1+\beta)}{2c_0^2\rho_0} \ll 1. \quad (4.8)$$

The result is much similar to that found in Eq. (4.7), except that $\phi_1 = -\frac{ip_1}{\omega\rho_0(1+i\Gamma)^2}$. Note that by neglecting the viscosity, Eq. (4.8) simplifies to Eq. (4.7) as is to be expected. The conclusion drawn from Eq. (4.8), is that even though viscosity is included, but $\nabla^2 \mathbf{v}_1 = \nabla(\nabla \cdot \mathbf{v}_1)$ for e.g. a standing one-dimensional-wave $\cos(kz)$, Eq. (4.6) still holds true for both ρ_1 , p_1 , ϕ_1 and \mathbf{v}_1 .

4.1.1 The general representation of the velocity field and thermoviscous and viscous boundary layers

For completeness, we will make a brief remark on how to account for viscous and thermoviscous boundary layers. When accounting for viscosity, one has to be careful when operating with the Laplacian, since according to the Helmholtz decomposition, the velocity field can in general be decomposed into the gradient of a scalar potential ϕ and the rotation of a divergence free vector potential ψ ,

$$\mathbf{v}_1 = \nabla\phi + \nabla \times \psi, \quad \text{with} \quad \nabla \cdot (\nabla \times \psi) = 0, \quad \nabla \times \nabla\phi = \mathbf{0}. \quad (4.9)$$

In general the complete expression of the Laplacian Eq. (2.3c) and velocity field Eq. (4.9) needs to be taken into consideration, in order to find solutions to an acoustofluidic system. To do this, the Navier–Stokes equation, Eq. (4.3b), is divided into a compressional component containing $\nabla\phi_1$ and p_1 , and a rotational component containing $\nabla \times \psi$.

Through appropriate boundary conditions, Karlsen and Bruus find the length of the two viscous boundary layers to be giving by

$$\delta = \sqrt{\frac{2\nu_0}{\omega}}, \quad \delta_t = \sqrt{\frac{2D_t}{\omega}}, \quad \text{with} \quad \nu_0 = \frac{\eta_0}{\rho_0}, \quad D_t = \frac{k_t}{\rho_0 c_p}, \quad (4.10)$$

where ν_0 is the momentum diffusion constant and D_t is the thermal diffusion constant given by the thermal conductivity k_t and specific heat capacity c_p .

Whenever we analyze a system a distance $r \geq 5\delta, 5\delta_t$ away from a boundary with boundary layers, we use the term “bulk”. The same restriction applies to suspended particles ($r \rightarrow a$), in order to ignore the thermoviscous and viscous effects. For a slightly more detailed discussion, see Appendix B.1.1

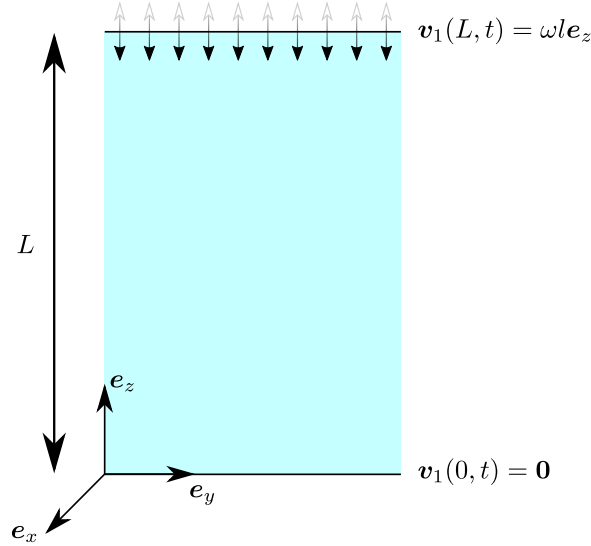


Figure 4.1: Two infinite parallel rigid walls, of which the top one is vibrating and the bottom is stationary, enforcing boundary conditions on the first order velocity field. Note that the boundary condition at $z = L$ is in complete agreement with Eq. (4.11). The white and black double arrows indicate direction of vibration. The vibrating amplitude is $l \ll L$ allowing us to consider the position of the walls fixed in time.

4.2 Solutions to Helmholtz wave equation for an ideal levitator

In Chapter 6 we find the exact analytical expression for the acoustic radiation force for the ideal single-axis levitator. However, the derivation depends on the solutions to Helmholtz wave equation in such a levitator system. In this section we will present the solution at resonance, where viscosity is accounted for in the bulk of a fluid, which eventually allows us to interpret the meaning and definition of an inviscid fluid. The derivation of the solution is very similar to that of Ref. [18], and a thorough treatment is found in Appendix B.2.

Consider two planar parallel rigid walls at $z = 0$ and $z = L$ that spans the entire xy -plane, see Fig. 4.1. Let the spacing of length L between them, be filled with a fluid and the bottom wall be completely stationary (hard wall condition). The top wall is vibrating at angular frequency ω and amplitude l , where $l \ll L$, such that we can neglect the actual displacement of the top wall. The time derivative of the position at the stationary and vibrating walls evidently represents boundary conditions on the first-order velocity field,

$$\mathbf{v}_1(0, t) = \mathbf{0}, \quad \text{and} \quad \mathbf{v}_1(L, t) = \omega l \mathbf{e}_z \quad (4.11)$$

The top wall acts as the acoustic generator, that actuates acoustic waves in the system. The acoustic waves are then reflected on the bottom wall, and at resonance we hit

the system's acoustic eigenmode, and the acoustic resonance builds up, until it becomes stationary in a steady-state.

Due to the simplicity and symmetry of the single-axis levitator, it is evident that the velocity field is one-dimensional, with only a z -dependency, i.e. $\mathbf{v}_1(z, t) = v(z)e^{-i\omega t}\mathbf{e}_z$. Thus, $\nabla \times \mathbf{v}_1 = \mathbf{0}$, and by Eq. (2.3c) we find $\nabla^2 \mathbf{v}_1 = \nabla(\nabla \cdot \mathbf{v}_1)$. By solving Eq. (4.6) at resonance, and making various expansions - see Appendix B.2, we find

$$\phi_1(z, t) \approx (-1)^n c_0 l \left(\frac{i}{n\pi\Gamma} \cos\left(n\pi \frac{z}{L}\right) + \frac{z}{L} \sin\left(n\pi \frac{z}{L}\right) \right) e^{-i\omega_n t}, \quad (4.12a)$$

$$\mathbf{v}_1(z, t) \approx (-1)^n \omega_n l \left(\frac{-i}{n\pi\Gamma} \sin\left(n\pi \frac{z}{L}\right) + \frac{z}{L} \cos\left(n\pi \frac{z}{L}\right) \right) e^{-i\omega_n t} \mathbf{e}_z, \quad (4.12b)$$

where at resonance, the wavenumber is given as

$$k_0 = k_n = n \frac{\pi}{L} = \frac{\omega}{c_0}, \quad \text{with } n = 1, 2, 3, \dots \quad (4.13)$$

$p_1(z, t)$ and $\rho_1(z, t)$ can subsequently be calculated by Eq. (4.8) and Eq. (4.1). We additionally define the n th angular frequency at resonance,

$$\omega_n = n \frac{\pi c_0}{L}. \quad (4.14)$$

It should be stressed that the resonant angular frequencies ω_n , in Eq. (4.14), are not exact, but exceptionally good approximations as $k_0 \Gamma L \ll 1$. Assuming typical values for a levitator setup containing air, we find in Table 4.2 $k_0 \approx 700$, and hence $L \approx 1/2$ cm. This allows us to calculate $k_0 \Gamma_{\text{air}} L \approx 2 \times 10^{-4} \ll 1$.

Since the amplitude of the resonant component is far bigger than the off-resonant, we can for practical purposes in relation to the acoustic radiation force, neglect the off-resonant part. The physical argument being that during a full oscillation cycle the resonant component will completely dominate the off-resonance. A more thorough and mathematical argumentation is found in Appendix B.3.

Consequently, the eigenmodes drive the single-axis levitator at resonance, and Eq. (4.12) can further be simplified by neglecting all non-resonant components,

$$\phi_1(z, t) \approx i(-1)^n \frac{c_0 l}{n\pi\Gamma} \cos(k_n z) e^{-i\omega_n t}, \quad (4.15a)$$

$$\mathbf{v}_1(z, t) \approx i(-1)^{n-1} \frac{lc_0}{L\Gamma} \sin(k_n z) e^{-i\omega_n t} \mathbf{e}_z. \quad (4.15b)$$

Note that Eq. (4.15) satisfies Eqs. (4.6) and (4.7) for the inviscid case $k = k_0 = \frac{\omega}{c_0}$ and $\eta_0 = 0$,

$$\nabla^2 \mathbf{v}_1 = -k_0^2 \mathbf{v}_1, \quad \nabla^2 \phi_1 = -k_0^2 \phi_1, \quad \nabla^2 p_1 = -k_0^2 p_1. \quad (4.16)$$

This is an important result, since the inviscid Helmholtz wave equation Eq. (4.16) contains no information about viscosity. However, the derived resonant acoustic waves, which are limited by the fluids viscosity, are solutions to Eq. (4.16). Clearly, this must be a major part of the interpretation of inviscid fluids.

For completeness we write the acoustic energy density which is derived in Appendix B.4 by following Ref. [18]. The derivation of time harmonic oscillating systems, involves spatial integrations of twice the time-averaged kinetic energy density,

$$E_{\text{ac}}(\omega) = \frac{\rho_0 \omega^2 l^2}{4n^2 \pi^2} \frac{\omega_n^2}{(\omega - \omega_n)^2 + \Gamma^2 \omega_n^2} \quad (4.17)$$

Eq. (4.17) emphasises the importance of including the viscosity, when analysing any fluid regardless of the viscosity magnitude. It is the viscosity that limits both the acoustic energy density and the amplitude of the system's eigenmodes. This leads to the interpretation of the term “inviscid fluid”. Naturally, the term does not imply diverging energies nor diverging eigenmodes. “Inviscid fluid” refers to the neglect of viscous boundary layers, expressing the dampening factor as part of an amplitude, e.g. $v_a = \frac{\omega_n l}{n\pi\Gamma}$, and more importantly, that the acoustic waves solve the inviscid Helmholtz wave equation, Eq. (4.16). Accompanying this, we henceforth consider the acoustic waves in an ideal levitator, as a solution to the inviscid Helmholtz wave equation with a fixed amplitude.

This leads to expressing the energy density at resonance in terms of said amplitude,

$$E_{\text{ac}} = \frac{\rho_0 \omega_n^2 l^2}{4n^2 \pi^2 \Gamma^2} = \frac{\rho_0}{4} v_a^2, \quad \text{at resonance.} \quad (4.18)$$

Furhter analysis of Eq. (4.17) shows that, when $\omega = \omega_n \pm \Gamma\omega_n$ the acoustic energy density $E_{\text{ac}}(\omega)$ is at half maximum, letting us write the full width at half maximum as $\Delta\omega = 2\Gamma\omega_n$. By definition, the quality factor Q , which is a measure of energy stored in the system divided by energy dissipated per cycle, of the resonance become,

$$Q = 2\pi \frac{\text{Energy stored}}{\text{Energy dissipated per cycle}} = \frac{\omega_n}{\Delta\omega} = \frac{1}{2\Gamma} \quad (4.19)$$

4.3 Physical parameters

For future use, two tables of physical parameters of interest should be presented. Table 4.1 lists the values of relevant quantities for this thesis. Note that the specific heat capacity k_t and thermal conductivity c_p , which are related to thermoviscous effects, are included for the sake of calculating the thermoviscous boundary width.

Table 4.1: Physical parameters at ambient pressure and temperature 0.1 MPa and 300 K, respectively, for air and water. These values are found in Refs. [11, 23] and citations therein.

Parameter	Symbol	Air	Water	Units
Speed of sound ^a	c_0	3.474×10^2	1.502×10^3	m s^{-1}
Density of mass	ρ_0	1.161	9.966×10^2	kg/m^3
Compressibility ^a	κ_0	7.137×10^{-6}	4.451×10^{-10}	Pa^{-1}
Shear viscosity	η_0	1.854×10^{-5}	8.538×10^{-4}	Pa s
Bulk viscosity	η^b	1.1×10^{-5}	2.4×10^{-3}	Pa s
Specific heat capacity	c_p	1.007×10^3	4.181×10^3	$\text{J kg}^{-1} \text{K}^{-1}$
Thermal conductivity	k_t	2.638×10^{-2}	6.095×10^{-1}	$\text{W m}^{-1} \text{K}^{-1}$

^aFor an adiabatic system

Other parameters mentioned throughout this chapters are calculated in Table 4.2, using values from Table 4.1.

Table 4.2: Relevant calculated parameters for a system perturbed by acoustic fields with frequency $f = 40$ kHz, using Table 4.1.

Parameter	Symbol	Air	Water	Units
Viscous ratio	β	9.266×10^{-1}	–	–
Dampening factor ^c	Γ	3.203×10^{-5}	–	–
Inviscid wavenumber	k_0	7.235×10^2	–	m^{-1}
Viscous boundary width	δ	1.1276×10^{-5}	–	m
Thermoviscous boundary width	δ_t	1.340×10^{-5}	–	m

^cUnderestimated

4.3.1 Final notes on the Quality factor

We will end this chapter with a few final notes on the quality factor, since the dampening factor Γ calculated in Table 4.2 is underestimated at best, and hence the quality factor is overestimated. In real experiments, where the fluid is encapsulated by boundary walls,

boundary layers will emerge. Thus, the energy dissipation through the bulk viscosity alone, cannot explain what is observed. In reality the energy predominantly dissipates in the viscous boundary layers by shear motion and heat conduction into the walls. A correction to this discrepancy can be made through averaging all contributions to heat dissipation as an overall viscous effect throughout the entire fluid.

Due to this uncertainty of the averaged dampening factor, the analytically calculated acoustic amplitudes are difficult to properly estimate. However, the amplitudes are in reality easily adjusted and tuned, simply through actuation. Thus, we will henceforth omit explicitly expressing the acoustic field's amplitude in terms of the dampening factor and simply use ρ_a , ϕ_a , p_a and v_a whenever appropriate.

Chapter 5

Acoustic radiation force exerted on small particles

When solving the Helmholtz wave equation in Chapter 4 with time harmonic solutions, the Navier–Stokes equation Eq. (4.3b), reveals that no first-order acoustic field will be able to produce any time-averaged forces. An elastic solid or droplet suspended in an acoustofluidic system with only time harmonic acoustic fields, would effectively not experience any acoustic forces during the short oscillation period $T = 1/f$, with f being of order many kHz. However, stable forces acting on a suspended elastic solid or droplet in fluids, have been observed in experiments, such as those made by Xie and Wei [15]. In order to find the acoustic radiation force, we have to resort to second-order perturbation theory for which time harmonic solutions are not assumed. As previously, the starting point will be the Navier–Stokes and continuity equations.

5.1 Second-order perturbation theory

Just as in Section 4.1, we will follow the notation of Ref. [18], when deriving the second order Navier–Stokes and continuity equations. However, we will go straight to the inviscid case for the purpose of this thesis.

In order to perform second-order perturbation theory we extend Eq. (4.1) with a second order term,

$$p = p_0 + p_1 + p_2 \quad \rho = \rho_0 + \rho_1 + \rho_2, \quad \mathbf{v} = \mathbf{0} + \mathbf{v}_1 + \mathbf{v}_2. \quad (5.1)$$

Performing yet another Taylor expansion of the pressure $p(\rho)$ in ρ around ρ_0 , we arrive at,

$$p(\rho) = p_0 + c_0^2(\rho_1 + \rho_2) + \frac{1}{2}(\partial_p c_0^2)\rho_1^2, \quad \text{where} \quad p_2 = c_0^2\rho_2 + \frac{1}{2}(\partial_p c_0^2)\rho_1^2. \quad (5.2)$$

Substituting Eqs. (5.1) and (5.2) into Eqs. (2.13b) and (2.7), and only look for terms of second order, as the first-order equations are accounted for, we find,

$$\partial_t \rho_2 = -\rho_0 \nabla \cdot \mathbf{v}_2 - \nabla \cdot (\rho_1 \mathbf{v}_1), \quad (5.3a)$$

$$\rho_0 \partial_t \mathbf{v}_2 = -\nabla p_2 - \rho_1 \partial_t \mathbf{v}_1 - \rho_0 (\mathbf{v}_1 \cdot \nabla) \mathbf{v}_1. \quad (5.3b)$$

We now introduce $\langle \mathbf{v} \rangle$ as the time average over a full oscillation cycle,

$$\langle \mathbf{v}(t) \rangle \equiv \frac{1}{T} \int_0^T dt \mathbf{v}(t), \quad (5.4)$$

and note that a time-averaged time harmonic field is zero, and a product of a two time harmonic fields does not average to zero. Additionally, in a steady oscillating system, such as investigated in this thesis, the second order fields contain a time harmonic component and a steady component. Consequently, the time derivative of a second order field becomes time harmonic, and so also average to zero with respect to time.

Consequently, by taking the time average of Eq. (5.3), we arrive at

$$\rho_0 \nabla \cdot \langle \mathbf{v}_2 \rangle = -\nabla \cdot \langle \rho_1 \mathbf{v}_1 \rangle, \quad (5.5a)$$

$$\nabla \langle p_2 \rangle = -\langle \rho_1 \partial_t \mathbf{v}_1 \rangle - \rho_0 \langle (\mathbf{v}_1 \cdot \nabla) \mathbf{v}_1 \rangle, \quad (5.5b)$$

and in order to proceed, we use the inviscid first-order continuity and Navier–Stokes equations found in Section 4.1,

$$\partial_t \rho_1 = -\rho_0 \nabla \cdot \mathbf{v}_1, \quad (5.6a)$$

$$\rho_0 \partial_t \mathbf{v}_1 = -\nabla p_1. \quad (5.6b)$$

When substituting Eq. (5.6b) into Eq. (5.5b), and recall that $\mathbf{v}_1 = \nabla \phi_1 = \frac{1}{i\omega\rho_0} \nabla p_1$, and note that $\frac{1}{2} \nabla \langle v_1^2 \rangle = \langle (\mathbf{v}_1 \cdot \nabla) \mathbf{v}_1 \rangle$ (for inviscid fluids) and $\frac{1}{2} \nabla \langle p_1^2 \rangle = \langle p_1 \nabla p_1 \rangle$, Eq. (5.5b) reduces to

$$\langle p_2 \rangle = \frac{1}{2} \kappa_0 \langle p_1^2 \rangle - \frac{1}{2} \rho_0 \langle v_1^2 \rangle, \quad (5.7)$$

where $\kappa_0 = \frac{1}{\rho_0 c_0^2}$ is the adiabatic compressibility found in Section 4.1. It is well known, that the real part of the time-average of a product of two time harmonic fields, $f(\mathbf{r}, t) = F(\mathbf{r})e^{-i\omega t}$ and $g(\mathbf{r}, t) = G(\mathbf{r})e^{-i\omega t}$, is given by

$$\langle f(\mathbf{r}, t)g(\mathbf{r}, t) \rangle = \frac{1}{2} \text{Re} [F(\mathbf{r})G^*(\mathbf{r})], \quad (5.8)$$

with asterix denoting complex conjugation.

5.2 The acoustic radiation force

If a fluid, upon which time harmonic acoustic fields are applied, is disturbed by an elastic solid or droplet of radius a , the acoustic waves will be scattered, and the elastic solid or droplet will experience an acoustic radiation force. This force must be equal to the change of momentum integrated across the surface. Hence, from Eq. (2.8) with $\partial\mathcal{V} \rightarrow \partial\Omega$ being the particle surface, neglecting body forces and ignoring viscosity, we find

$$\mathbf{F} = - \oint_{\partial\Omega} [p\mathbf{n} + \rho(\mathbf{n} \cdot \mathbf{v})\mathbf{v}] ds, \quad (5.9)$$

where \mathbf{n} is the surface unit vector directed outwards away from the particle surface $\partial\Omega$.

Taking the time average of Eq. (5.9) in order to find the purely acoustical radiation force, only second-order terms remains, and by inserting Eq. (5.7) into Eq. (5.9), we get

$$\begin{aligned}\langle \mathbf{F}^{\text{rad}} \rangle &= - \oint_{\partial\Omega} [\langle p_2 \rangle \mathbf{n} + \rho_0 \langle (\mathbf{n} \cdot \mathbf{v}_1) \mathbf{v}_1 \rangle] ds \\ &= - \oint_{\partial\Omega} \left[\left\{ \frac{1}{2} \kappa_0 \langle p_1^2 \rangle - \frac{1}{2} \rho_0 \langle v_1^2 \rangle \right\} \mathbf{n} + \rho_0 \langle (\mathbf{n} \cdot \mathbf{v}_1) \mathbf{v}_1 \rangle \right] ds.\end{aligned}\quad (5.10a)$$

For simplicity we will omit the explicit time-average notation of the radiation force, and it is thus implicit whenever we write \mathbf{F}^{rad} .

Evidently, Eq. (5.10) is expressed solely in terms of first-order acoustic fields. Denoting the incoming acoustic wave as ϕ_{in} and the scattered acoustic wave propagating away from the elastic solid or droplet as ϕ_{sc} , we can describe the total first-order acoustic fields as a sum of the two.

$$\phi_1 = \phi_{\text{in}} + \phi_{\text{sc}}, \quad (5.11a)$$

$$p_1 = p_{\text{in}} + p_{\text{sc}} = i\omega\rho_0 (\phi_{\text{in}} + \phi_{\text{sc}}), \quad (5.11b)$$

$$\mathbf{v}_1 = \mathbf{v}_{\text{in}} + \mathbf{v}_{\text{sc}} = \nabla (\phi_{\text{in}} + \phi_{\text{sc}}). \quad (5.11c)$$

Regardless of the form of the total acoustic fields, Eq. (5.10) expresses the radiation force.

In certain limits of the size of an elastic solid, the expression of the acoustic radiation force can be greatly simplified. By following the method of Gorkov [6], Settnes and Bruus [10] arrives at a two terms expression to zeroth order in the radius and viscous boundary ratio $\frac{\delta}{a}$, in the limit $a \ll \lambda$, where λ is the acoustic wavelength. By evaluating all acoustic fields at the center of the suspended particle, the acoustic radiation force is written as,

$$\mathbf{F}_{\text{sa}}^{\text{rad}} = -\pi a^3 \left[\frac{2\kappa_0}{3} \text{Re} [f_0^* p_{\text{in}}^* \nabla p_{\text{in}}] - \rho_0 \text{Re} [f_1^* \mathbf{v}_{\text{in}}^* \cdot \nabla \mathbf{v}_{\text{in}}] \right] \quad \text{in general,} \quad (5.12a)$$

or

$$\mathbf{F}_{\text{sa}}^{\text{rad}} = -\nabla U_{\text{sa}}^{\text{rad}} \quad \text{for a standing wave } \phi_{\text{in}}, \quad (5.12b)$$

$$U_{\text{sa}}^{\text{rad}} = \frac{4\pi}{3} a^3 \left(f_0 \frac{\kappa_0}{2} \langle p_{\text{in}}^2 \rangle - f_1 \frac{3\rho_0}{4} \langle v_{\text{in}}^2 \rangle \right), \quad \text{if } \delta \ll a, \quad (5.12c)$$

where “sa” denotes the case of small radius $a \ll \lambda$, also referred to as the small argument, and where we introduced the monopole f_0 and dipole f_1 scattering coefficients,

$$f_0 = 1 - \tilde{\kappa}, \quad \text{and} \quad f_1 = \frac{2(\tilde{\rho} - 1)}{2\tilde{\rho} + 1}. \quad (5.12d)$$

In Eq. (5.12) we further introduced the ratios $\tilde{\kappa} = \frac{\kappa_p}{\kappa_0}$ and $\tilde{\rho} = \frac{\rho_p}{\rho_0}$, where κ and ρ are the compressibility and density respectively, and subscripts “p” and “0” refers to the elastic

solid and ambient fluid respectively. The strength of Eq. (5.12), is that it only contains a monopole and a dipole term, as higher modes are neglectable, and that it only depends on the incoming acoustic fields, making physical predictions much simpler.

It should be noted that Settles and Bruus work is not limited to inviscid cases only. Their work covers the general case, where the viscous boundary layers can no longer be neglected.

In case of a suspended droplet rather than an elastic solid, there is in general a differentiation between the two. The droplet cannot carry an acoustic shear wave and the droplet also have an internal viscous boundary layer δ' , due to the droplet's internal viscosity η' . Karlsen and Bruus [11] show that the difference presents itself by a correction of the scattering coefficients f_0 and f_1 , i.e. calculating the radiation force to first-order in $\frac{\delta'}{a}$. However, since we investigate the inviscid case, we will no longer distinguish between droplets or elastic solids in this thesis, and we simply refer to either one as a particle.

Now assume that the applied acoustic field is a standing wave, $p_{\text{in}} = p_0 \cos(k_0 z) \sin(\omega t)$, where $k_0 = 2\pi/\lambda = \omega/c_0$ is the usual wavenumber, the acoustic radiation force reduces to,

$$\mathbf{F}_{\text{sa}}^{\text{rad}} = 4\pi\Phi(\tilde{\kappa}, \tilde{\rho})k_0 a^3 E_{\text{ac}} \sin(2k_0 z) \mathbf{e}_z, \quad a \ll \lambda \quad (5.13)$$

which is shown by Bruus in Ref. [12]. Further, in Eq. (5.13) we find the acoustic energy density $E_{\text{ac}} = (p_0^2)/(4\rho_0 c_0^2)$, and we introduced the so-called contrast factor in terms of the monopole and dipole coefficients, $\Phi(\tilde{\kappa}, \tilde{\rho}) = \frac{1}{3}f_0(\tilde{\kappa}) + \frac{1}{2}f_1(\tilde{\rho})$. As briefly discussed in Chapter 1, Eq. (5.13) is especially interesting in relation to the levitator. When balancing the acoustic radiation force with the gravitational body force of a spherical particle, $\mathbf{F}_{\text{body}} = \mathbf{F}_{\text{g}} = -\frac{4}{3}\pi\rho_p a^3 g \mathbf{e}_z$, both forces are proportional with the particle radius cubed. Consequently, the levitating properties of a particle is independent of particle size, and solely depend on the actuated amplitude and position. However, for larger particles the levitating position is expected to pick up a size dependency.

Hence, a more general study of the incoming and scattered acoustic waves is necessary.

5.3 The general wave expansion

Where Eq. (5.12) perfectly describes the radiation force in terms of the monopole and dipole coefficients in the small particle limit, in the larger particle limit, higher modes are likely to become significant, which we will explicitly show in Chapter 6.

However, in order to evaluate the significance of higher modes, and to derive an exact expression for the radiation force, it will prove valuable to solve the inviscid Helmholtz wave equation [Eq. (4.16)], with wavenumber k_0 in spherical coordinates. The solution is standard textbook material, and by avoiding singular solutions at $r = 0$, and considering outgoing scattered waves, it is written in terms of spherical Bessel functions $j_n(k_0 r)$, the outgoing spherical Hankel functions $h_n(k_0 r)$ and Legendre polynomials $P_n \cos \theta$. Further, since we, with no exception, deal with azimuthal symmetry, there is no φ dependency around the axis, which is convenient in regards to the single-axis levitator. This approach requires us to account for the transmitted compressional wave ϕ_c , that propagates inside

the particle. This wave being the only one that is transmitted in the inviscid case. Hence, we write the solutions:

In the fluid, $r > a$

$$\phi_{\text{in}} = \phi_0 \sum_{n=0}^{\infty} i^n (2n+1) j_n(k_0 r) P_n(\cos \theta) = \phi_0 e^{-ik_0 z}, \quad (5.14a)$$

$$\phi_{\text{sc}} = \phi_0 \sum_{n=0}^{\infty} i^n (2n+1) A_n h_n(k_0 r) P_n(\cos \theta). \quad (5.14b)$$

In the particle, $r < a$

$$\phi_c = \phi_0 \sum_{n=0}^{\infty} i^n (2n+1) A'_n j_n(k_p r) P_n(\cos \theta), \quad (5.14c)$$

where ϕ_0 is an arbitrary wave amplitude with unit $\text{m}^2 \text{s}^{-1}$, A_n and A'_n are complex coefficients determined by appropriate boundary conditions. k_p is the wavenumber inside the particle equivalent to the fluid wavenumber k_0 . The time dependency, $e^{-i\omega t}$, is implicit in Eq. (5.14). We will in general adopt this notation and let the time dependency be implicit for all subsequent expressions of the acoustic fields.

The boundary conditions for the inviscid fluid for sufficiently small oscillations are

$$v_{1r} = v'_{1r}, \quad \sigma_{rr} = \sigma'_{rr}, \quad \text{at } r = a, \quad (5.15)$$

where superscript prime denotes particle domain. The above-mentioned conditions are determined by the fact, that the radial particle oscillation must follow that of the fluid, as there are no limits to the transverse motion of the fluid around the particle. Additionally, the stress must be continuous across the boundary in the radial direction. Otherwise, a finite change in stress across an infinitesimal distance would result in an infinite force.

By adopting the notation of Karlsen and Bruus, we introduce the dimensionless wavenumbers $x = k_0 a$ and $x_p = k_p a$ for the fluid and particle respectively, the two boundary conditions at the particle surface are,

$$a v_{1r} = a v'_{1r}$$

$$\phi_0 \sum_{n=0}^{\infty} i^n (2n+1) P_n(\cos \theta) [x j'_n(x) + A_n x h'_n(x) - A'_n x_p j'_n(x_p)] = 0, \quad (5.16a)$$

$$\sigma_{rr} = \sigma'_{rr}$$

$$\phi_0 \sum_{n=0}^{\infty} i^n (2n+1) P_n(\cos \theta) [\rho_0 j_n(x) + \rho_0 A_n h_n(x) - \rho_p A'_n j'_n(x_p)] = 0. \quad (5.16b)$$

Through straightforward calculation, and by utilizing the orthogonality of the Legendre polynomials, one finds the coefficients A_n in terms of A'_n to be

$$A_n = \tilde{\rho} \frac{A'_n j_n(x_p)}{h_n(x)} - \frac{j_n(x)}{h_n(x)}, \quad (5.17)$$

where,

$$A_n = -\frac{j_n(x)}{h_n(x)} \left\{ \frac{1 - \tilde{\rho} \tilde{c} \frac{j_n(\frac{x}{\tilde{c}}) j'_n(x)}{j_n(x) j'_n(\frac{x}{\tilde{c}})}}{1 - \tilde{\rho} \tilde{c} \frac{j_n(\frac{x}{\tilde{c}}) h'_n(x)}{h_n(x) j'_n(\frac{x}{\tilde{c}})}} \right\}, \quad (5.18)$$

is expressed in terms of x and $\tilde{c} = \frac{k_0}{k_p} = \frac{c_p}{c_0}$ as $x_p = \frac{x}{\tilde{c}}$. We only explicitly write the scattering coefficients A_n as they make up the scattered wave in the ambient fluid, and hence are included in the radiation force expression through Eq. (5.10). A'_n can subsequently be found by Eq. (5.17).

It is noteworthy that the scattering coefficients A_n are determined by the physical material ratios \tilde{c} and $\tilde{\rho}$, and depends on the free variable $x = k_0 a$, i.e. applied frequency and particle radius. Since, in the small particle limit ($x \ll \pi$), the radiation force contains a monopole and dipole coefficient, we can calculate the two first modes $n = 0$ and $n = 1$ in the small particle limit, where A_0 and A_1 simplifies to (see Appendices C.1 and C.2 for full derivation),

$$A_0|_{x \ll \pi} = -\frac{ix^3}{3} (1 - \tilde{\kappa}) = -\frac{ix^3}{3} f_0, \quad (5.19a)$$

$$A_1|_{x \ll \pi} = \frac{ix^3}{6} \frac{2(\tilde{\rho} - 1)}{2\tilde{\rho} + 1} = \frac{ix^3}{6} f_1. \quad (5.19b)$$

Clearly, A_n must be directly related to the acoustic radiation force. It also, and more importantly, indicate that Eq. (5.12) cannot remain a good approximation as $x \rightarrow \pi$, i.e. $a \rightarrow \frac{\lambda}{2}$ (note that there is no upper limit on x as it depends not only on particle size but also on frequency. This limit is chosen as the second lowest resonant frequency and largest particle size). Graphically, see Fig. 5.1, we can conclude that higher modes than $n = 1$ will become relevant in terms of their magnitude, additionally the x^3 -scaling of the dominating scattering coefficients cannot remain a good approximation. Fig. 5.1(a) indicates that it is very likely, that just as A_0 and A_1 emerge as part of the acoustic radiation force, higher modes of the acoustic radiation force may become relevant as well, but Fig. 5.1(b) indicates that the predominant change is the scaling and hence the complete representation of the A_n coefficients. Motivated by this, we will in next chapter calculate an exact expression of the acoustic radiation force, where all modes will be accounted for.

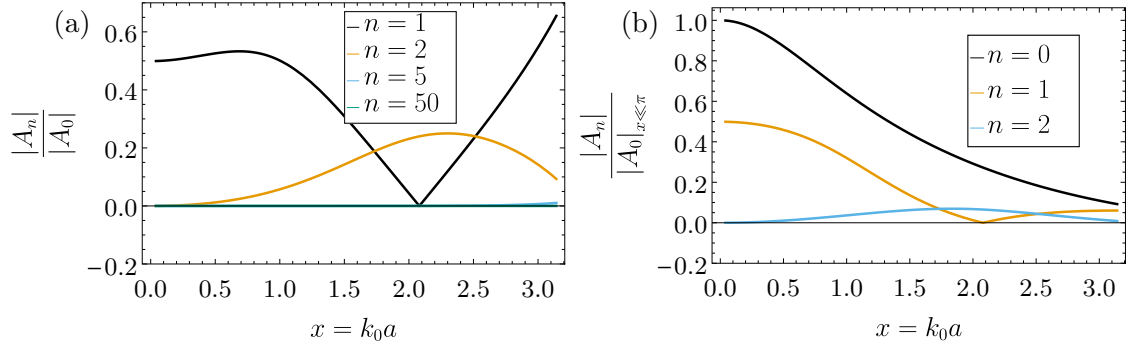


Figure 5.1: Values from Table 4.1 are used to calculate $\tilde{\rho}$ and \tilde{c} . Absolute values of the scattering coefficient are used, as we do not yet know exactly how these coefficient are expressed in the acoustic radiation force. (a) The ratio between the scattering coefficient A_0 and coefficients of higher modes, $n = 1$, $n = 2$, $n = 5$, and $n = 50$ plotted as function of the dimensionless wavenumber x . It is clear that, as $x \rightarrow \pi$ higher modes become of same order of magnitude as lower orders and cannot be ignored. (b) The ratio between the small argument scattering coefficient $A_0|_{x \ll \pi}$ and coefficients of higher modes, $n = 0$, $n = 1$, and $n = 2$ plotted as function of the dimensionless variable x . It is evident that the dominating scattering coefficient no longer can be assumed to scale as x^3 as $x \rightarrow \pi$.

Chapter 6

Acoustic radiation force exerted on large particles

In this chapter, we will derive an analytical expression for the exact radiation force and balance it with the force of gravity for a spherical particle, \mathbf{F}_g , to find positions of acoustic levitation. Our starting point will be the time-averaged acoustic radiation force evaluated on a spherical particle,

$$\mathbf{F}^{\text{rad}} = - \oint_{\partial\Omega} \left[\left\{ \frac{1}{2} \kappa_0 \langle p_1^2 \rangle - \frac{1}{2} \rho_0 \langle v_1^2 \rangle \right\} \mathbf{n} + \rho_0 \langle (\mathbf{n} \cdot \mathbf{v}_1) \mathbf{v}_1 \rangle \right] ds. \quad (6.1)$$

6.1 Exact acoustic radiation force from a standing wave

Consider an applied incoming standing pressure wave and the corresponding velocity- and potential fields oscillating around the z -axis. If then, the system is perturbed by a particle of radius a , the particle experiences a force given by Eq. (6.1), integrated at the particle surface. Letting the origin of the applied acoustic waves coincide with the center of the particle, see Fig. 6.1, we write the acoustic waves in terms of $\tilde{z} = z - z_0$, such that $z = \tilde{z} + z_0$.

We divide the acoustic velocity potential into its respective exponential parts,

$$\phi_{\text{in}} = c_\phi (\phi_{\text{in}}^+ \pm \phi_{\text{in}}^-), \quad \phi_{\text{in}}^+ = \phi_0 e^{ik_0 z} = \phi_0 e^{ik_0(\tilde{z} + z_0)} = (\phi_{\text{in}}^-)^*, \quad (6.2a)$$

where $c_\phi = \{\pm 1, \pm i\}$ is a constant meant to ensure the correct relation between pressure and the velocity potential, and $k_0 = \frac{c_0}{\omega_0}$ being the usual wavenumber. The velocity field and pressure field are found the usual way,

$$\mathbf{v} = \nabla \phi_{\text{in}}, \quad p_{\text{in}} = i\omega \rho_0 \phi_{\text{in}}. \quad (6.2b)$$

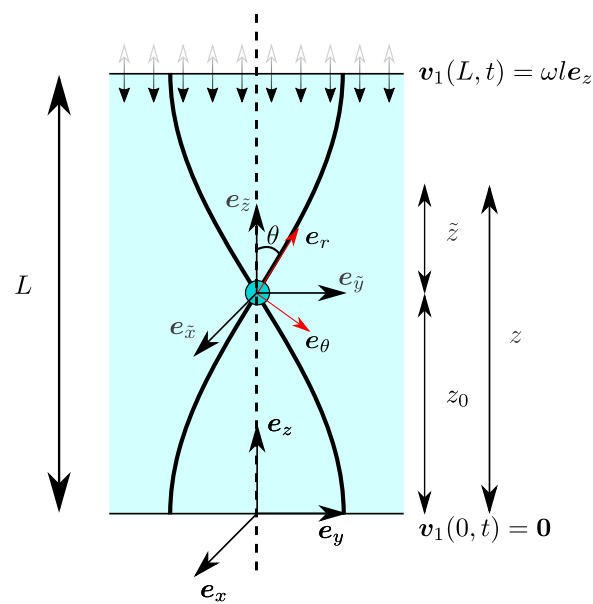


Figure 6.1: A suspended particle (cyan) at $z = z_0$, in a standing acoustic pressure wave, ρ_1 at resonance, actuated by the top vibrating rigid wall. This levitator is ideal meaning that the rigid bottom wall and rigid vibrating top wall span the entire xy -plane. Additionally, the velocity boundary conditions are the same as those described in Section 4.2. The origins of both the cartesian and the spherical coordinate systems are indicated by the corresponding unit vectors, black and red respectively. Note that \tilde{z} is some position measured in the “tilde” coordinate system, which in terms of z is written as $\tilde{z} = z - z_0$.

Using the general spherical solution to Helmholtz wave equation Eq. (5.14) (where we perform the spherical expansion in “tilde” coordinates) and the scattering coefficients Eq. (5.18), we write,

$$\phi_1 = \phi_{\text{in}} + \phi_{\text{sc}}, \quad (6.3a)$$

where,

$$\phi_{\text{in}} = c_\phi \phi_0 \sum_{n=0}^{\infty} i^n (2n+1) j_n(k_0 r) \left[e^{ik_0 z_0} \pm (-1)^n e^{-ik_0 z_0} \right] P_n(\cos \theta), \quad (6.3b)$$

$$\phi_{\text{sc}} = c_\phi \phi_0 \sum_{n=0}^{\infty} i^n (2n+1) A_n h_n(k_0 r) \left[e^{ik_0 z_0} \pm (-1)^n e^{-ik_0 z_0} \right] P_n(\cos \theta). \quad (6.3c)$$

Hence,

$$\phi_1 = c_\phi \phi_0 \sum_{n=0}^{\infty} i^n (2n+1) \left\{ j_n(k_0 r) + A_n h_n(k_0 r) \right\} \left[e^{ik_0 z_0} \pm (-1)^n e^{-ik_0 z_0} \right] P_n(\cos \theta). \quad (6.3d)$$

Let ϑ_n and the vector potential function Φ , not to be confused with the contrast factor from Chapter 5, be given as,

$$\vartheta_n = e^{ik_0 z_0} \pm (-1)^n e^{-ik_0 z_0} \quad (6.4a)$$

$$\Phi(k_0 r)_n = \phi_0 i^n (2n+1) \left\{ j_n(k_0 r) + A_n h_n(k_0 r) \right\}, \quad [\Phi] = \text{m}^2 \text{s}^{-1}. \quad (6.4b)$$

Using the derived relations between ϕ , \mathbf{v} and p , we further define the pressure function, S (S as an indication of stress associated with pressure), radial- and angular- velocity functions, V_r and V_θ respectively,

$$S(k_0 r)_n = \omega \rho_0 \Phi(k_0 r)_n, \quad [S] = \text{Pa}, \quad (6.4c)$$

$$V_r(k_0 r)_n = \partial_r \Phi(k_0 r)_n, \quad [V_r] = \text{m s}^{-1}, \quad (6.4d)$$

$$V_\theta(k_0 r)_n = \frac{\Phi(k_0 r)_n}{r}, \quad [V_\theta] = \text{m s}^{-1}. \quad (6.4e)$$

With this we write compact expressions for ϕ_1 , $p_1 = i\omega \rho_0 \phi_1$ and $\mathbf{v}_1 = \nabla \phi_1$,

$$\phi_1 = c_\phi \sum_{n=0}^{\infty} \Phi(k_0 r)_n \vartheta_n P_n(\cos \theta) \quad (6.5a)$$

$$p_1 = i c_\phi \sum_{n=0}^{\infty} S(k_0 r)_n \vartheta_n P_n(\cos \theta), \quad (6.5b)$$

$$v_{1r} = c_\phi \sum_{n=0}^{\infty} V_r(k_0 r)_n \vartheta_n P_n(\cos \theta), \quad (6.5c)$$

$$v_{1\theta} = c_\phi \sum_{n=0}^{\infty} V_\theta(k_0 r)_n \vartheta_n \partial_\theta P_n(\cos \theta), \quad (6.5d)$$

where subscript “1 r ” and “1 θ ” denotes radial and angular component respectively.

This and using Eq. (5.8) allows us to rewrite the individual parts in Eq. (6.1) by noting that the constant c_ϕ evaluates to one through products of $c_\phi c_\phi^* = 1$ by time-averaging

$$\langle p_1^2 \rangle = \frac{1}{2} \text{Re} [p_1 p_1^*] = \sum_{n,m} \frac{1}{2} \text{Re} [S(k_0 r)_n S^*(k_0 r)_m \vartheta_n \vartheta_m^* P_n(\cos \theta) P_m(\cos \theta)], \quad (6.6a)$$

where $\{n, m\} \geq 0$, and similarly,

$$\langle v_1^2 \rangle = \frac{1}{2} \text{Re} [v_{1r} v_{1r}^*] + \frac{1}{2} \text{Re} [v_{1\theta} v_{1\theta}^*], \quad (6.6b)$$

$$\langle (\mathbf{n} \cdot \mathbf{v}_1) \mathbf{v}_1 \rangle = \frac{1}{2} \text{Re} [v_{1r} v_{1r}^*] \mathbf{e}_r + \frac{1}{2} \text{Re} [v_{1\theta} v_{1\theta}^*] \mathbf{e}_\theta. \quad (6.6c)$$

Using the results, Eq. (6.6a) - Eq. (6.6c) and Eq. (6.5b) - Eq. (6.5d), we find each contribution to the radiation force Eq. (6.1), when integrating over the particle surface, to be,

$$\oint_{\partial\Omega} \left[\frac{1}{2} \kappa_0 \langle p_1^2 \rangle \mathbf{n} \right] ds = \sum_{m,n} \frac{a^2 \pi}{2} \kappa_0 \text{Re} [S(x)_n S^*(x)_m \vartheta_n \vartheta_m^* L_{nm}] \mathbf{e}_z, \quad (6.7a)$$

$$\begin{aligned} - \oint_{\partial\Omega} \left[\frac{1}{2} \rho_0 \langle v_1^2 \rangle \mathbf{e}_r \right] ds &= - \sum_{m,n} \frac{a^2 \pi}{2} \rho_0 \text{Re} [V_r(x)_n V_r^*(x)_m \vartheta_n \vartheta_m^* L_{nm}] \mathbf{e}_z \\ &\quad - \sum_{m,n} \frac{a^2 \pi}{2} \rho_0 \text{Re} [V_\theta(x)_n V_\theta^*(x)_m \vartheta_n \vartheta_m^* I_{n,m}] \mathbf{e}_z, \end{aligned} \quad (6.7b)$$

$$\begin{aligned} \oint_{\partial\Omega} [\rho_0 \langle (\mathbf{e}_r \cdot \mathbf{v}_1) \mathbf{v}_1 \rangle] ds &= \sum_{n,m} a^2 \pi \rho_0 \text{Re} [V_r(x)_n V_r^*(x)_m \vartheta_n \vartheta_m^* L_{nm}] \mathbf{e}_z \\ &\quad + \sum_{n,m} a^2 \pi \rho_0 \text{Re} [V_r(x)_n V_\theta^*(x)_m \vartheta_n \vartheta_m^* B_{n,m}] \mathbf{e}_z. \end{aligned} \quad (6.7c)$$

where $x = k_0 a$ is the dimensionless variable introduced in Chapter 5, and ds indicates surface integral. When evaluating each of these integrals, the angular dependency of the Legendre polynomials and the unit vectors, $\mathbf{e}_r = \sin(\theta) \cos(\phi) \mathbf{e}_x + \sin(\theta) \sin(\phi) \mathbf{e}_y + \cos \theta \mathbf{e}_z$ and $\mathbf{e}_\theta = \cos \theta \cos(\phi) \mathbf{e}_x + \cos \theta \sin(\phi) \mathbf{e}_y - \sin(\theta) \mathbf{e}_z$, need to be accounted for. However, only terms, other than the ones containing \mathbf{e}_z due to the rest evaluating to zero, when integrating with respect to ϕ , remain. Hence, we simply allow the following substitutions $\mathbf{e}_r \rightarrow \cos \theta \mathbf{e}_z$ and $\mathbf{e}_\theta \rightarrow -\sin(\theta) \mathbf{e}_z$. Evidently, we only have to calculate three different cases in order to find the relation between index m and n ,

$$L_{nm} = \int_{-1}^1 P_n(y)P_m(y)P_1(y) dy \mathbf{e}_z = \begin{cases} \frac{2n}{(2n+1)(2n-1)} \mathbf{e}_z = L_n^- \mathbf{e}_z, & \text{if } m = n - 1 \\ \frac{2(n+1)}{(2n+3)(2n+1)} \mathbf{e}_z = L_n^+ \mathbf{e}_z, & \text{if } m = n + 1, \\ 0, & \text{else} \end{cases} \quad (6.8a)$$

$$I_{n,m} = \int_{-1}^1 C_{n-1}^{3/2}(y)C_{m-1}^{3/2}(y)C_1^{1/2}(y) (1 - y^2) dy \quad (6.8b)$$

$$= \begin{cases} \frac{\pi \prod_{a=1}^3 [\Gamma(J-l_a - \frac{1}{2})] (J+1)!}{4\Gamma(1/2)^2 \Gamma(3/2)^2 \Gamma(J+3/2) (J-n)! (J-m)! (J-2)!}, & \text{if } m = n \pm 1 \text{ and } m + n \geq 3, \\ 0, & \text{else} \end{cases}$$

$$B_{n,m} = \int_{-1}^1 C_n^{1/2}(y)C_{m-1}^{3/2}(y) (1 - y^2) dy \quad (6.8c)$$

$$= \begin{cases} \frac{\pi (-1)^{\frac{m-n+1}{2}} (m+1)! \Gamma(J - \frac{1}{2})}{4(m-1)! \Gamma(1/2) \Gamma(3/2) \Gamma(J+3/2) (J-n)! (J-m)!} \mathbf{e}_z, & \text{if } m = n \pm 1 \text{ and } m \geq 1, \\ 0, & \text{else} \end{cases}$$

where $J = \frac{1}{2}(n + m + 1)$, $l_a = \{l_1, l_2, l_3\} = \{n, m, 1\}$, and we substituted $y = \cos \theta$ and introduced the more general Gegenbauer polynomials, $C_n^\lambda(y)$, of which the Legendre polynomials are special cases, namely $P_n(y) = C_n^{1/2}(y)$ [24]. Differentiating the Legendre polynomials yields yet another type of Gegenbauer polynomials [25], which has also been used to obtain Eq. (6.8). The actual integration is made by identification and comparison with the work done by S. Alisauskas [26] and Y. Hagiwara [27]. A more detailed calculation of Eq. (6.8), and how they relate to Eq. (6.7), is found in Appendix D.1.

Applying these integrals, allows us to calculate the exact acoustic radiation force exerted on a spherical particle with radius $a = x/k_0$, in a fluid with parameters, ρ_0 and κ_0 ,

$$\begin{aligned}
\mathbf{F}_{\text{exact}}^{\text{rad}} = & -\frac{1}{2} \frac{x^2}{k_0^2} \pi \mathbf{e}_z \left\{ \kappa_0 \left(\sum_{n=1}^{\infty} L_n^- \text{Re} [S(x)_n \vartheta_n S^*(x)_{n-1} \vartheta_{n-1}^*] \right. \right. \\
& \left. \left. + \sum_{n=0}^{\infty} L_n^+ \text{Re} [S(x)_n \vartheta_n S^*(x)_{n+1} \vartheta_{n+1}^*] \right) \right. \\
& + \rho_0 \left(\sum_{n=1}^{\infty} L_n^- \text{Re} [V_r(x)_n \vartheta_n V_r^*(x)_{n-1} \vartheta_{n-1}^*] \right. \\
& \left. + \sum_{n=0}^{\infty} L_n^+ \text{Re} [V_r(x)_n \vartheta_n V_r^*(x)_{n+1} \vartheta_{n+1}^*] \right) \\
& - \rho_0 \left(\sum_{n=2}^{\infty} I_{n,n-1} \text{Re} [V_\theta(x)_n \vartheta_n V_\theta^*(x)_{n-1} \vartheta_{n-1}^*] \right. \\
& \left. + \sum_{n=1}^{\infty} I_{n,n+1} \text{Re} [V_\theta(x)_n \vartheta_n V_\theta^*(x)_{n+1} \vartheta_{n+1}^*] \right) \\
& + 2\rho_0 \left(\sum_{n=2}^{\infty} B_{n,n-1} \text{Re} [V_r(x)_n \vartheta_n V_\theta^*(x)_{n-1} \vartheta_{n-1}^*] \right. \\
& \left. \left. + \sum_{n=0}^{\infty} B_{n,n+1} \text{Re} [V_r(x)_n \vartheta_n V_\theta^*(x)_{n+1} \vartheta_{n+1}^*] \right) \right\}. \quad (6.9)
\end{aligned}$$

Notice, how every mode n couples with another mode $n \pm 1$, and so each term in Eq. (6.9) will contain one of the possible combination of $\vartheta_n \vartheta_{n\pm 1}^* = (e^{ik_0 z} \pm e^{-ik_0 z}) (e^{-ik_0 z} \mp e^{ik_0 z})$. Consequently, we find that

$$\begin{aligned}
\vartheta_n \vartheta_{n\pm 1}^* & = (e^{ik_0 z_0} \pm e^{-ik_0 z_0}) (e^{-ik_0 z_0} \mp e^{ik_0 z_0}) = \mp (e^{ik_0 z_0} + e^{-ik_0 z_0}) (e^{ik_0 z_0} - e^{-ik_0 z_0}) \\
& = \mp 4i \cos(k_0 z_0) \sin(k_0 z_0) = \mp i 2 \sin(2k_0 z_0). \quad (6.10a)
\end{aligned}$$

Eq. (6.10) yields same position dependency of the particle as found in Eq. (5.13), as $\text{Re} [(a + ib)i \sin(2k_0 z_0)] = \sin(2k_0 z_0) \text{Re} [(a + ib)i]$ for some real numbers a and b .

We will denote the finite sum of the radiation force as $\mathbf{F}_{\text{exact}}^{\text{rad}}|_{\infty \rightarrow N}$. What is noteworthy, is that through the defined functions $S(x)$, $V_r(x)$ and $V_\theta(x)$, the scattering coefficients A_n couples with modes one higher and one lower. Recalling that A_0 and A_1 both appear in the small argument radiation force $\mathbf{F}_{\text{sa}}^{\text{rad}}$ through Eq. (5.19), we could suspect that modes up to $N = 2$ need to be included, when calculating the exact radiation to leading order for $x \ll \pi$. We will in later sections see, that this is indeed the case.

6.2 Resultant forces from an acoustic standing wave

Eq. (6.9) allows us to calculate the exact radiation force for any kind of applied standing acoustic wave, and any value of $x \gg \delta, \delta_t$, in an assumed inviscid fluid. Since both $\mathbf{F}_{\text{exact}}^{\text{rad}}$ and $\mathbf{F}_{\text{sa}}^{\text{rad}}$ only are directed in the z -direction, we will usually omit specifying them as vectors, and simply write $F_{\text{exact}}^{\text{rad}}$ and $F_{\text{sa}}^{\text{rad}}$ respectively.

By placing a particle in the ideal levitator setup analysed in Section 4.2, see Fig. 6.1, the resulting real expressions for the pressure-, velocity- and potential fields whose origin coincide with the origin of the particle are

$$p_{\text{in}} = p_a \cos(k_0(\tilde{z} + z_0))e^{-i\omega t} = \frac{1}{2}p_a \left(e^{ik_0(\tilde{z}+z_0)} + e^{-ik_0(\tilde{z}+z_0)} \right) e^{-i\omega t}, \quad (6.11)$$

$$\phi_{\text{in}} = \frac{1}{2} \frac{p_a}{i\omega\rho_0} \left(e^{ik_0(\tilde{z}+z_0)} + e^{-ik_0(\tilde{z}+z_0)} \right) e^{-i\omega t}, \quad (6.12)$$

$$\mathbf{v}_{\text{in}} = \frac{1}{2} \frac{p_a}{i\omega\rho_0} \nabla \left(e^{ik_0(\tilde{z}+z_0)} + e^{-ik_0(\tilde{z}+z_0)} \right) e^{-i\omega t}, \quad (6.13)$$

where $\tilde{z} = z - z_0$ is the position measured along the z -axis, from the origin of the particle.

Thus, by comparison with Eq. (6.2), we identify $c_\phi = -i$ and $\phi_0 = \frac{1}{2} \frac{p_a}{\omega\rho_0}$, consequently letting us write the acoustic radiation force as expressed in Eq. (6.9).

Consider now a water particle placed in a single-axis levitator, such that it is suspended in air as in Fig. 6.1 at $z_0 = \pi/(4k_0)$, at which Eq. (5.13) hits an anti-node, thus producing the largest magnitude of acoustic force. In order to calculate the radiation force, we assume that the levitator dimensions ensures that we reach resonance, i.e.

$$L = n \frac{\pi c_0}{\omega_n} = n \frac{c_0}{2f_n} = n \frac{\lambda_n}{2}, \quad (6.14)$$

where f_n is the n th frequency of resonance for a given ideal levitator system. The relevant physical parameters in the inviscid case are listed in Table 4.1.

If we apply acoustic fields with frequency $f_1 = 40 \times 10^3$ Hz, assume $p_a = 1$ Pa (for simplicity, as p_a is divided out, whenever we divide by E_{ac}), and let \tilde{c} , $\tilde{\rho}$ and $\tilde{\kappa}$ denote the ratios of speed of sound, density of mass and compressibility as in Section 5.2, we can compare Eq. (6.9) and Eq. (5.13) graphically by plotting,

$$\frac{F_{\text{exact}}^{\text{rad}}}{F_{\text{sa}}^{\text{rad}}} = \frac{F_{\text{exact}}^{\text{rad}}}{4\pi\Phi(\tilde{\kappa}, \tilde{\rho})k_0 \left(\frac{x}{k_0}\right)^3 E_{\text{ac}} \sin(2k_0 z)}. \quad (6.15)$$

The result has two major implications as seen in Fig. 6.2(a). First of all, we see that in order to account for the full radiation force in the small particle limit, it is necessary to include up to mode $N = 2$. However, when doing so we find total agreement in the small particle limit as $F_{\text{exact}}^{\text{rad}} \rightarrow F_{\text{sa}}^{\text{rad}}$ for $x \rightarrow 0$. Secondly, we see that $F_{\text{exact}}^{\text{rad}} \leq F_{\text{sa}}^{\text{rad}}, \forall x$ and that the force changes direction compared to $F_{\text{sa}}^{\text{rad}}$, when including modes up to $N = 50$, around $x \sim 1.9$.

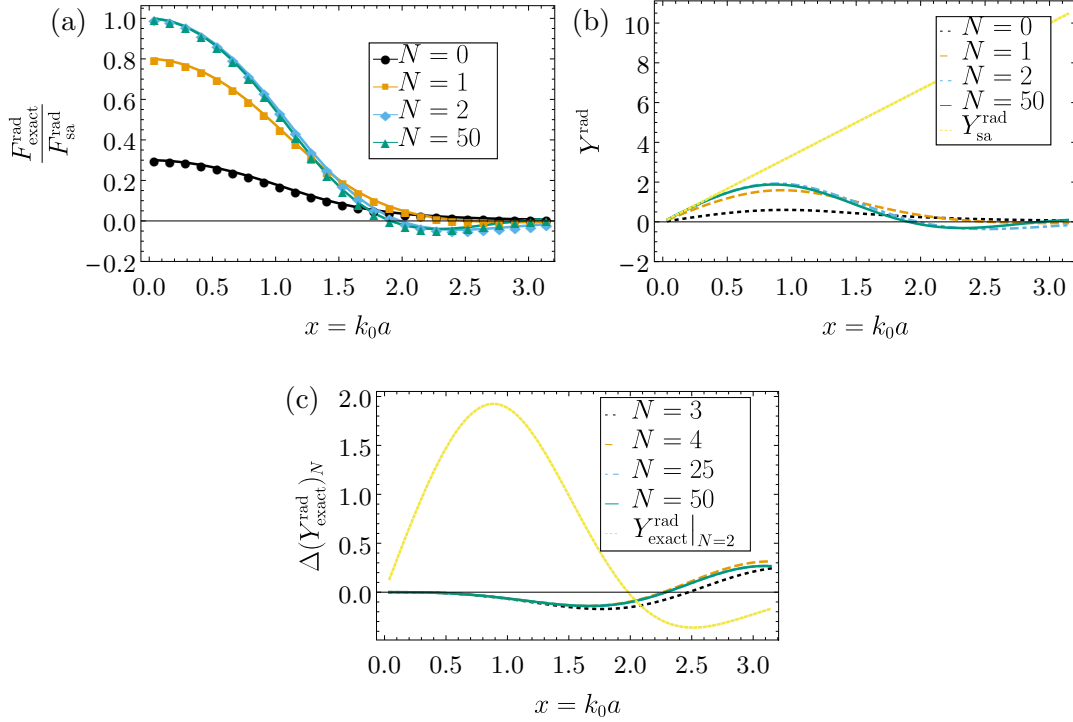


Figure 6.2: (a) The relation between the small argument radiation force derived by Settes and Bruus [10] and the exact radiation force, where modes up to $N = 0$ (black), $N = 1$ (orange), $N = 2$ (blue) and $N = 50$ (green) are included as a function of the dimensionless parameter x . (b) The radiation force function as a function of the dimensionless parameter x for modes included up to $N = 0$, $N = 1$, $N = 2$, $N = 50$ and $Y_{\text{sa}}^{\text{rad}}$ for comparison. (c) The difference between $Y_{\text{exact}}^{\text{rad}}|_{N=2}$ and $Y_{\text{exact}}^{\text{rad}}|_{N>2}$ as a function of the dimensionless parameter x for modes included up to $N = 3$, $N = 4$, $N = 25$, $N = 50$ and $Y_{\text{exact}}^{\text{rad}}|_{N=2}$ (yellow) for visual comparison to compare orders of magnitude.

In relation to balancing the force of gravity \mathbf{F}_g , with the acoustic radiation force, it is important to analyze how $F_{\text{exact}}^{\text{rad}}$ scales with x as $x \rightarrow \pi$ in order to predict stable positions of levitation. To do so we introduce the dimensionless radiation force function Y^{rad} , as inspired by Hasegawa and Yosioka [28]. The radiation force function is defined as

$$Y_i^{\text{rad}} = \frac{F_i^{\text{rad}}}{\sin(2k_0 z_0) E_{\text{ac}} \pi a^2}, \quad \text{where } i = \text{exact, sa}, \quad (6.16)$$

and E_{ac} is the time averaged acoustic energy density for a standing wave, and z_0 denotes the vertical position of the water particle. The radiation force function can be plotted as a function of the dimensionless quantity x . A comparison of $Y_{\text{exact}}^{\text{rad}}$ and $Y_{\text{sa}}^{\text{rad}}$ emphasizes the change of scaling, when using the exact representation of the acoustic radiation force, as $F_{\text{sa}}^{\text{rad}} \propto x^3$. Fig. 6.2(b) illustrates how $F_{\text{exact}}^{\text{rad}} \not\propto x^3$ for $x \rightarrow \pi$, and so balancing the force of gravity with the radiation force varies with particle size as well as position. We can

also conclude from Fig. 6.2(a) & (b), that for large enough x the force of gravity F_g will outscale $F_{\text{exact}}^{\text{rad}}$ throughout the entire levitator domain, and hence the single-axis levitator will no longer be stable.

We are yet to determine the importance of including higher modes, when calculating $F_{\text{exact}}^{\text{rad}}$. To do this, we need to look at Fig. 6.2(c), which show the difference $(\Delta Y_{\text{exact}}^{\text{rad}})_N = Y_{\text{exact}}^{\text{rad}}|_{N=2} - Y_{\text{exact}}^{\text{rad}}|_{N>2}$. What we find, graphically, is that higher modes do indeed contribute to the total radiation force, and whether we include modes up to $N = 25$ or $N = 50$, makes little difference. Additionally, the importance of higher modes becomes more significant as $x \rightarrow \pi$, but when comparing (b) and (c), we conclude that including the exact expressions for the scattering coefficients A_n become significant earlier than including higher modes. As a final note to this, it would be interesting to derive how many modes that are necessary to include, to get a certain accuracy for a certain range of x . However, a quantitative treatment of this subject will not be made in thesis.

6.3 Levitating a particle

So far, we have discussed the differences between $F_{\text{exact}}^{\text{rad}}$ and $F_{\text{sa}}^{\text{rad}}$. Following this, we now aim at getting a better geometric and physical idea of how the $F_{\text{exact}}^{\text{rad}}$ varies in space, as well as where to find stable positions of levitation. Hence, we look at Fig. 6.3, which shows the magnitude of $F_{\text{exact}}^{\text{rad}}|_{N=25} / (E_{\text{ac}}\pi a^2)$ as a density plot on top of which a vectorplot indicates it's direction for two different values of x , $x = 4.078 \times 10^{-1}$ and $x = \frac{3}{2}\pi$. Since $F_{\text{exact}}^{\text{rad}}$ is an expression developed for an ideal single axis levitator, only the z_0 coordinate of the particle position, described in terms of x_0, y_0, z_0 (where x_0 is not the dimensionless wavenumber), is relevant. Hence, for the first-axis in Fig. 6.3 we plot y_0 as to not make further confusion with the dimensionless wavenumber x .

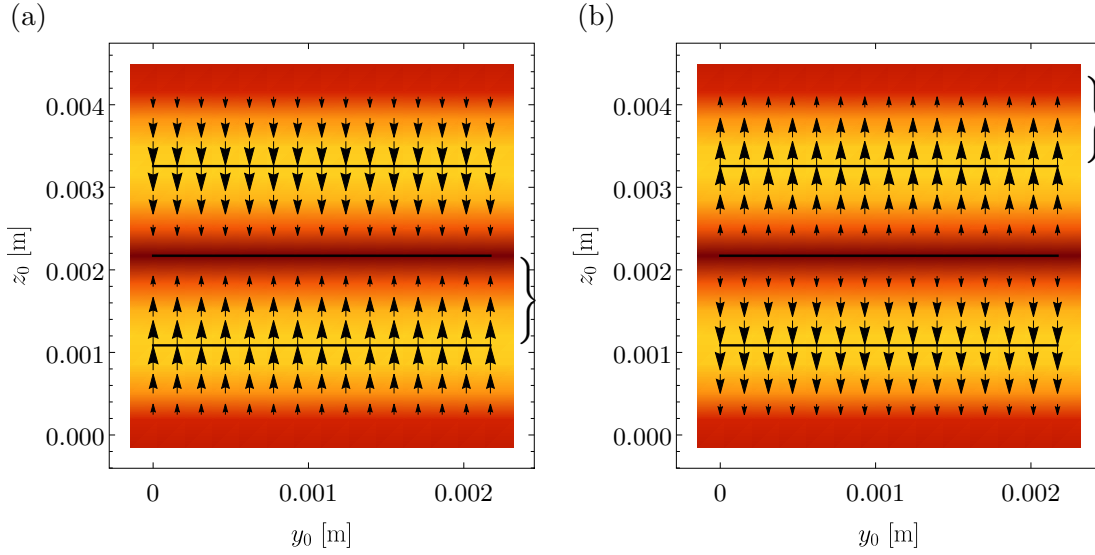


Figure 6.3: Vector density plot of the absolute value of $F_{\text{exact}}^{\text{rad}}|_{N=25} / (E_{\text{ac}}\pi a^2)$ shown in an ideal single-axis levitator, pictured in Fig. 6.1. The graphical results are a two-dimensional cross-section of an ideal levitator. The magnitude scale ranges in (a), zero (black) to 1.25 (yellow), (b) zero (black) to 0.25 (yellow). Each graph is calculated for different values of x , (a) $x = 4.078 \times 10^{-1}$ and (b) $x = \frac{3}{2}\pi$. The horizontal black lines mark the vertical particle position at $z_0 = \pi/(4k_0)$ (anti-node), $z_0 = \pi/(2k_0)$ (node) and $z_0 = 3\pi/(4k_0)$ (anti-node). The curly brackets indicate regions where $\partial_{z_0}(F_{\text{exact}}^{\text{rad}})_z < 0$, and thus may contain possible stable positions of levitation.

Fig. 6.3 serves to illustrate possible stable positions of levitation. The only possible position are those where $F_{\text{exact}}^{\text{rad}} = -F_g$. However, we need to impose another restriction, namely $\partial_{z_0}(F_{\text{exact}}^{\text{rad}})_z < 0$, such that a particle placed close to such a point, will fall into it. We notice that (a) and (b) show opposite directed forces, which we will return to later, why that is. Hence, the only candidates of stable position are for (a) in the region $\pi/(4k_0) < z_0 < \pi/(2k_0)$ and for (b) $3\pi/(4k_0) < z_0 < \pi/k_0$ indicated by curly brackets.

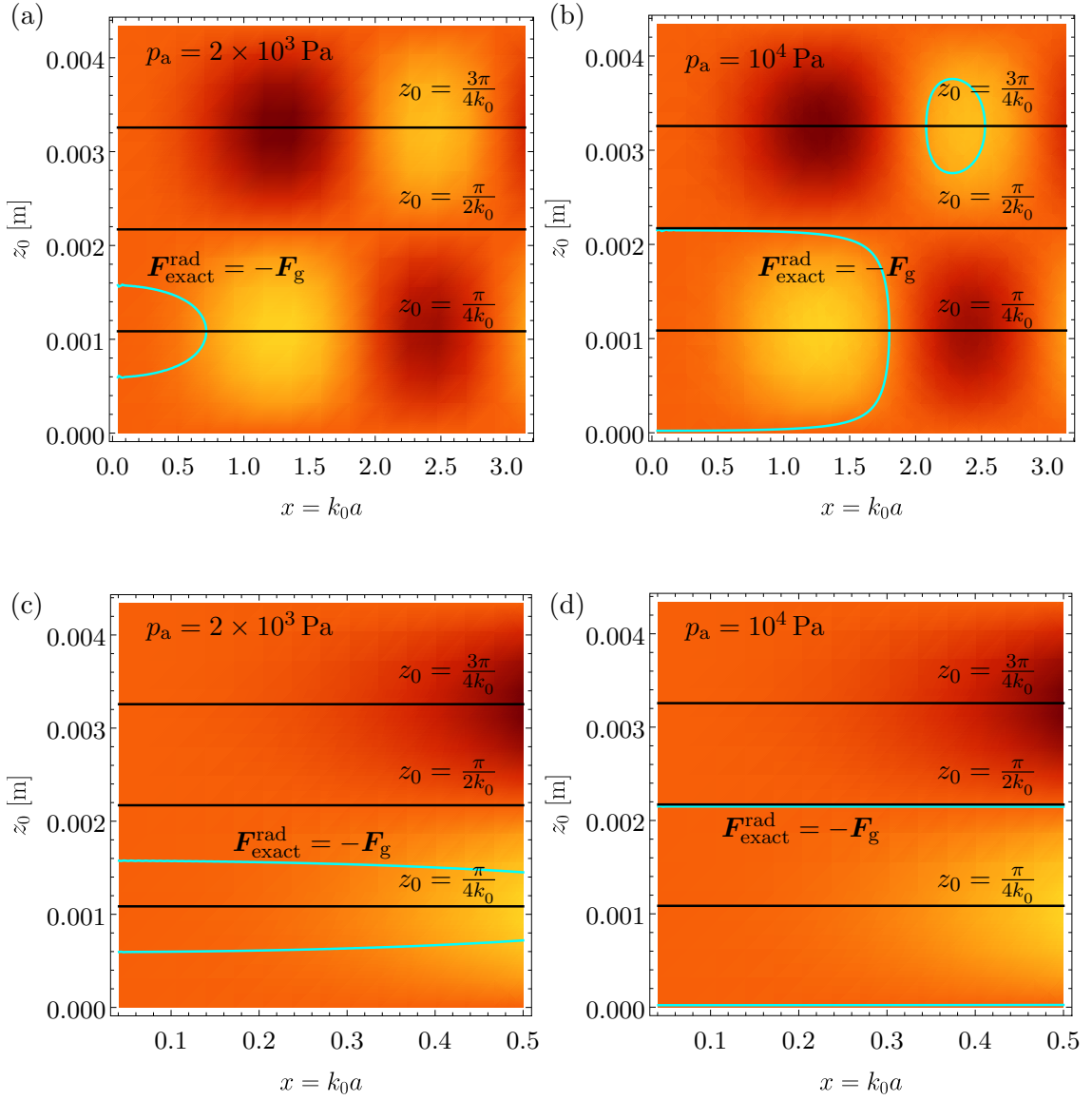


Figure 6.4: Balancing the force of gravity with the acoustic radiation force (cyan) to levitate a particle as a function of particle placement z_0 and wavenumber x with $p_0 = 2 \times 10^3$ Pa and $p_0 = 10^4$ Pa. The background shows a density plot of $F_{\text{rad}}^{\text{exact}}$. Notice how for larger values of x we see the position of levitation crawls towards the antinode. The magnitude ranges for each graph as, (a) -7.5×10^{-5} N (black) to 7.5×10^{-5} N (yellow), (b) $< -2 \times 10^{-3}$ N (black) to 2×10^{-3} N (yellow), (c) $< -1.5 \times 10^{-5}$ N (black) to 1.5×10^{-5} N (yellow) and (d) $< -3 \times 10^{-4}$ N (black) to 3×10^{-4} N. The horizontal black lines mark $z_0 = \pi/(4k_0)$, $z_0 = \pi/(2k_0)$ and $z_0 = 3\pi/(4k_0)$.

We now wish to find stable positions of levitation, and in order to balance the force of gravity with the acoustic radiation force, we have chosen two different arbitrary values of the pressure wave amplitude, $p_a = 2 \times 10^3$ Pa and $p_a = 10^4$ Pa, both of which are within the restrictions of perturbation theory. Fig. 6.4 shows a densityplot of $F_{\text{exact}}^{\text{rad}}$, and the cyan lines indicates positions where $F_{\text{exact}}^{\text{rad}} = -F_g$. In (a) & (c), the acoustic amplitude is too small to provide stable levitating positions for $x \gtrsim 1$. The earlier-mentioned restriction for stable levitation, dictates that only the line above $z_0 = 3\pi/(4k_0)$ is stable. We also conclude that for larger x , the stable position crawls towards the antinode, until it hits the antinode at some critical value x_{crit} .

However, if the amplitude is larger as in (b) & (d), more interesting tendencies arises. Clearly, we see the same tendency as for (a) and (b) if $x \lesssim 1.9$, and due to the larger amplitude the stable position of levitation starts off further away from the antinode. But, as it is illustrated, the amplitude is large enough that new domains of stable levitation arises as $x \rightarrow \pi$. The acoustic radiation force completely changes direction, and if $x \gtrsim 1.9$, then $z_0 > 3\pi/(4k_0)$ will provide stable levitation position as marked by the cyanic line. Suspecting this might be caused by oscillations with respect to x , one recalls that both the oscillating spherical Hankel and Bessel functions are the building blocks of $F_{\text{exact}}^{\text{rad}}$. Hence, they would cause the acoustic radiation force to start oscillating with respect to wavenumber x . With no upper limits on x and noting, that the previous limit was artificially set for analytical purposes, we now allow $x \rightarrow 3\pi$ and change the amplitude back to $p_0 = 1$ Pa. The result is as suspected. Fig. 6.5 clearly illustrates such oscillating tendencies, where the radiation force function changes sign everytime x passes some critical values, possibly related to but certainly not equal to $n\pi/2$.

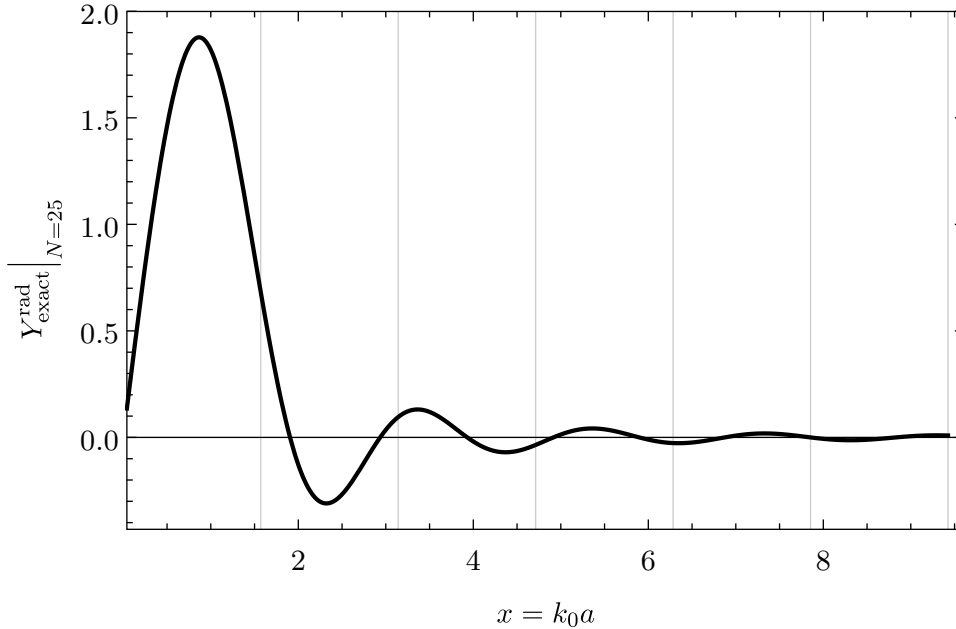


Figure 6.5: $Y_{\text{exact}}^{\text{rad}}|_{N=25}$ as a function of x . The vertical lines mark $x = n\pi/2$, $n \in \mathbb{N}$.

The reason for the oscillations arise from our loosely use of setting no upper restriction on x . It is true that x has no upper limit, but as x sweeps through certain values $x = m\pi/2$, $m \in \mathbb{N}$, the physical interpretation of the acoustic waves or levitator geometry changes. The allowed resonance frequencies for an ideal single axis-levitator is given by Eq. (6.14). Noting that for some levitator length L , the particle cannot be larger than $a = L/2$. However, we can still make x larger by considering one of the following two interpretations; either we maintain the same levitator geometry and apply a higher frequencies, such that $f_n = n\frac{c_0}{2L}$ or $\lambda_n = 2L/n$, or we maintain the same frequency, but apply it on another geometry, where $L_n = n\lambda/2$. The first interpretation implies $k_0 = k_n = nk_1 = n\pi/L$, which means that within the same levitator with length L , the acoustic radiation force oscillates n full times. The second interpretation implies moving the acoustic setup to another levitator geometry with length $L_{\text{new}} = n\lambda/2$, which again means, that within length L_{new} the acoustic radiation forces oscillates n full times. Consequently, every time x passes one of these values, we either consider the frequency to be larger or the geometry to become larger. Hence, Fig. 6.3, Fig. 6.4 and Fig. 6.5 belongs to the second interpretation (however each one is only plotted within $z_0 \leq \pi/k_0$, i.e. one full force oscillation), where $L = 3\lambda/2$ ($n = 3$), $L = \lambda$ ($n = 2$) and $L = \lambda/2$ ($n = 6$) respectively. Fig. 6.6 illustrates these different interpretations for x crossing the $m = 1$ mark.

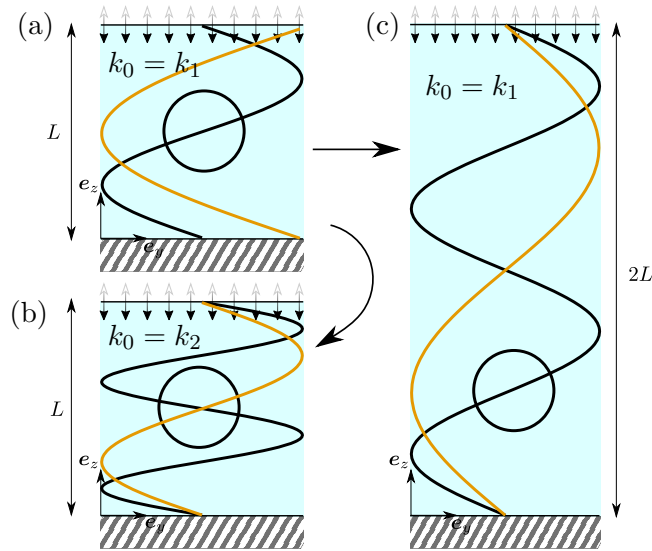


Figure 6.6: Illustration of interpreting the case where we allow $x \rightarrow \pi$ for an ideal levitator. In general the black line illustrates the radiation force, and the brown line represents the velocity field propagating in the direction of e_z . (a) is the starting point of a levitator with length L and lowest resonant wavenumber $k_0 = k_1$. (b) The interpretation of higher frequency, when $x > \pi/2$, where $k = k_2 = 2k_1$. (c) The interpretation, when $x > \pi/2$, where the levitator length is twice that of (a).

Regardless of choosing either of the interpretations, we would still see a change of force direction. However, Fig. 6.6 gives us an idea of why it may change. When $x = \pi/2$ we

find $d = 2a = \lambda/2$, which means that for even slightly larger x , we find $d > \lambda/2$, and so when integrating over the particle surface, we would also integrate over opposite directed velocity fields, compared to when $d < \lambda/2$. Further investigation is needed in order to make any proper conclusions, as the issue is not a simple one, due to the complex way the particle scatters and perturbs the acoustic fields. The first clue, indicating the complexity, is that the first change of force direction does not occur at $x = \pi/2$, but at $x \sim 1.9$.

The important results of this chapter are the necessity of including up to mode $N = 2$ in order for $F_{\text{exact}}^{\text{rad}}$ to fully amount to the acoustic force found by Settnes and Bruus. We then concluded that $F_{\text{exact}}^{\text{rad}} \propto x^3$ as $x \rightarrow \pi$, which is due to accounting for the full expression of the acoustic scattering coefficients A_n . For yet larger x , higher modes of $F_{\text{exact}}^{\text{rad}}$ become significant as well and must be included.

Related to the ideal single-axis levitator, the change of scaling, forces the stable positions of levitation, at first to crawl towards the acoustic force's anti-node. More interestingly, we find that the acoustic radiation force completely changes direction at certain critical values of x , due to an oscillation with respect to x .

These results can be applied, and should be considered, whenever an experimental single axis levitator can be assumed to actuate standing waves. One has to be careful, when tuning the oscillations and frequencies and the effects it has on the wavenumber x , in order to find desired levitation positions of a spherical particle.

6.4 Range of validity

In this thesis there are several possible restrictions that need to be addressed and evaluated. The first one being the validity of the perturbation theory which is only valid for

$$\epsilon_{\text{ac}} = \frac{|\rho_1|}{\rho_0} \ll 1, \quad (6.17)$$

where ϵ_{ac} is introduced as the perturbation parameter. Eq. (6.17) is not very restrictive, as the amplitudes of the applied acoustic fields are easily adjusted by actuation.

Secondly, as stated earlier in this thesis we assume particle radius much larger than δ , $a \gg \delta$, and with $f = 40$ kHz we find in Table 4.2 that $\delta = 2.825 \times 10^{-5}$ m. For the radius to be much larger than δ we demand $a \geq 5\delta = 5.636 \times 10^{-5}$ m leading to a limit on the dimensionless parameter $x \geq 4.078 \times 10^{-2}$.

However, there are three other assumptions which must be considered in order for the derived theory in this thesis to apply to any acoustofluidic experiment. The three being; the time periodicity, neglectable buoyancy force and small particle oscillations.

6.4.1 Time oscillation

Consideration to time periodicity is in general relevant whenever one investigates acoustofluidics, where flow is involved. It relates to non-zero time-averaged motion of particles, where the displacement during one oscillation cycle is small compared to particle radius. The phenomenon of drag, where drag forces are exerted on particles in fluids, due to the relative velocity between the flow of the ambient fluid and the particle, ought to be considered.

However, in case of the levitator, there can be assumed to be no flow in the ambient fluid and hence no drag force, and the particle follows the applied velocity field. The assumptions of time periodicity are thus exact, and we need not consider this further.

For a thorough discussion of time oscillation, see Ref. [11].

6.4.2 Boyancy force

The boyancy force exerted on a particle submerged in a fluid is standard textbook material, and it is opposite that of the force of gravity. Its magnitude is given as

$$F_{\text{boyancy}} = \rho_f V g, \quad (6.18)$$

where ρ_f is the density of the ambient fluid, V is the volume displaced by the particle and g is the acceleration of gravity. Since we completely neglect the force of boyancy but account for the force of gravity, we assume that,

$$\frac{F_{\text{boyancy}}}{F_g} = \frac{\rho_f V g}{\rho_p V g} = \frac{\rho_f}{\rho_p} \ll 1. \quad (6.19)$$

In the case of this thesis, where we investigate the single-axis levitator with a water droplet in air, we find that $\rho_{\text{air}}/\rho_{\text{water}} \approx 10^{-3}$ and thus Eq. (6.19) is non-restrictive.

6.4.3 Small particle oscillations

We have several times throughout this thesis made various evaluation right at the surface of the levitating particle, e.g. integration and formulating boundary conditions for the scattering coefficients A_n . However, in reality the radius of the particle is not constant in time, and its surface oscillates. Through the definition of the compressibility, we can estimate the maximum change of radius a_1 compared to the unperturbed radius a to be

$$\frac{a_1}{a} \simeq \frac{\kappa_p}{3} p_1 = \frac{\tilde{\kappa}}{3} \epsilon_{\text{ac}} \ll 1, \quad (6.20)$$

where $\kappa_0 p_1 = \epsilon_{\text{ac}}$ has been used. A thorough derivation is found in Appendix D.2. In case of the water droplet in air levitator, this is not a restriction, as $\tilde{\kappa} \ll 1$ and $\epsilon_{\text{ac}} \ll 1$. However, we evaluate the radiation force at the particle's position, described by its center of mass. Hence, the displacement of the particle's center of mass Δd relative to the particle radius in general has the following restriction, as argued by Karlsen and Bruus [11]

$$\frac{\Delta d}{a} \simeq \frac{\lambda}{2\pi a} \epsilon_{\text{ac}} \ll 1. \quad (6.21)$$

As with the other cases this is not severely restrictive, as we analyze fairly large particles ($a \geq 5.636 \times 10^{-5}$ m), such that $\epsilon_{\text{ac}} \ll 4.078 \times 10^{-2}$ must be fulfilled at frequency $f = 40$ kHz in order to be within the limit of Eq. (6.21). This is easily achievable through careful actuation.

Even though Karlsen's and Bruus work is based on particles smaller than the wavelength λ , their upper limit on the perturbation parameter still applies to this thises, where

we allow the levitating particle to be arbitrarily large. The reason being that we conclude, that the acoustic radiation force lessens as the particle becomes larger. Consequently, a smaller force on a larger particle results in a smaller oscillation, which makes Eq. (6.21) an overestimated limit, meant to emphasize that our analysis in this thesis is not strongly restricted in any of the before-mentioned cases.

Chapter 7

Simulating a single-axis levitator

The previous chapters conclude the treatment of the exact acoustic radiation force. One last subject to touch upon, is how concave reflectors improves or amplifies real levitators as mentioned in Chapter 1, as well as finding stable positions of levitation in a more realistic levitator. To this end, a simple azimuthal symmetric model of a single-axis levitator has been generated in Comsol. The model has been adjusted by sweeping through five different reflectors, which surface can be mathematically described by the expression

$$h_{\text{ref}} = h_0 + sr^2, \quad (7.1)$$

where $s = 0, 25, 50, 75, 100$ with units $[s] = \text{m}^{-1}$, h_0 is the flat reflector position, and r is radius measured from the axis of symmetry. Fig. 7.1 illustrates the geometry in the two extrema of the parameter s .

The model is constructed such that the height of the levitator domain (enclosed by the actuator and reflector) meets the requirement $L = \lambda/2 = c_0/(f2)$, where $f = 40 \text{ kHz}$ i.e. we would expect to see a standing resonant wave in the z -direction close to the axis of symmetry.

When solving the inviscid Helmholtz wave equation Eq. (4.16) for an azimuthal symmetric system, where $s = 0$, and the boundary conditions on the actuator- and reflector-surfaces, are that of Section 4.2, the spatial solution at resonance comes out as

$$p(r, \theta, z) = p_A \cos(lz) e^{\pm i\theta n} J_n(\varrho r), \quad n \in \mathbb{N}, \quad (7.2)$$

where J_n is the regular Bessel function, $\varrho^2 = k_0^2 - l^2$, $l = m\pi/L$, $m \in \mathbb{N}$ and p_A some amplitude. Additionally $e^{\pm i\theta n}$ implies a superposition of the exponential functions. For the detailed derivation, please see Appendix E.1. The importance of Eq. (7.2) is that the acoustic energy is divided into a z -directional part and a r -directional part, which together make up the total acoustic wave. The total wavenumber k_0 , which hold information about the resonant frequency of the system, is given as $k_0^2 = l^2 + \varrho^2$. Since the wavenumber l associated with the z -direction, can be assumed to be close to the same wavenumber in the ideal levitator, i.e. $l = 4\pi^2 f^2 / c_0^2$, f_{res} for the entire system can only be expected to be higher. We will make no further analytical treatment of the azimuthal symmetry problem. It is simply meant to explain what will be observed, when analyzing the numerical results obtained by Comsol.

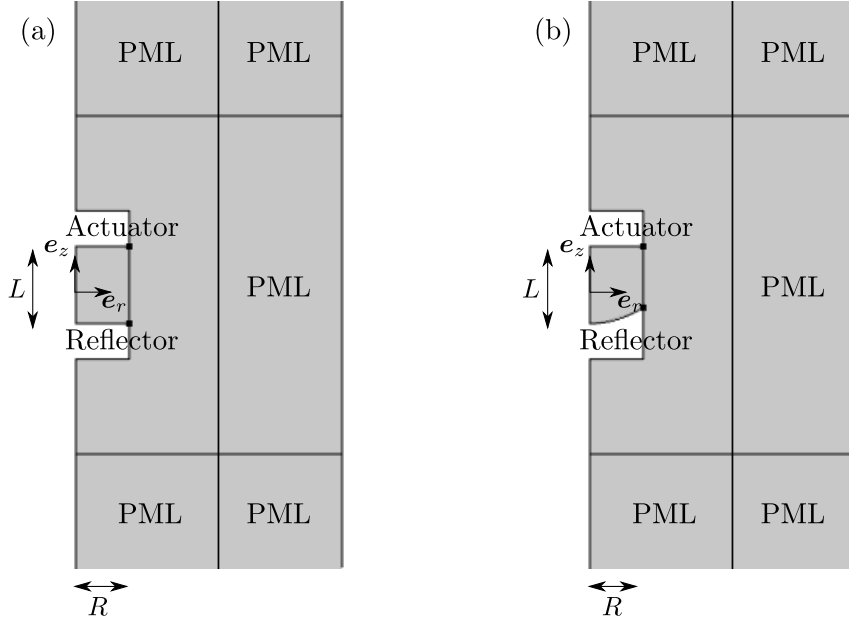


Figure 7.1: The two extrema geometries modelled in Comsol, where (a) $s = 0$ and (b) $s = 100$. The two white domain represent the actuator (top square) and reflector (bottom domain). The four outermost domains are Comsol’s implemented PML as mentioned in Chapter 3.

7.1 Setting up Comsol

This section briefly describes the used settings and boundary conditions applied in Comsol. As a physics module, the acoustic module, “Pressure Acoustics, Frequency Domain (acpr)” is applied on the entire domain of the geometry. As boundary conditions we specify all walls to be “hard wall”, i.e. that $(\mathbf{n} \cdot \nabla)p_1 = 0$. Along the entire far left line of Fig. 7.1 the axis of symmetry is specified, and on the bottom part of the actuator, we demand that $(\mathbf{n} \cdot \nabla)p_1 = (\mathbf{e}_z \cdot \nabla)p_1 = iv_{bc}$. In this case $v_{bc} = \omega d$, where $d = 6 \mu\text{m}$ is the small displacement of the actuator wall. Additionally, we only look for the solution in the case where $m = 0$ in Eq. (7.2), and hence we only find solutions for this special case, where the acoustic waves carry no azimuthal waves. This too is specified in Comsol. Finally, Comsol sweeps across frequencies from $f_{\text{applied}} = 40 \times 10^3 \text{ Hz}$ to $f_{\text{applied}} = 65 \times 10^3 \text{ Hz}$, to see if we hit the frequency of resonance. To do this, we calculate the general time-averaged acoustic energy density E_{ac} in the domain encapsuled by the levitator, such that

$$E_{ac} = \int_{\Omega} \left[\frac{\kappa_0 \langle p_1^2 \rangle}{2\mathcal{V}} + \frac{\rho_0 \langle v_1^2 \rangle}{2\mathcal{V}} \right] dV = \int_{\Omega} \left[\frac{\kappa_0 |p_1|^2}{4\mathcal{V}} + \frac{\rho_0 |v_1|^2}{4\mathcal{V}} \right] dV, \quad (7.3)$$

where \mathcal{V} is the volume encapsuled by the levitator of which we perform the integration. For various parameter values used to build the model and run the simulation, see Appendix E.2.

7.2 Results

The frequency response of the single-axis levitator build in Comsol, is just as expected. The resonant frequency is shifted to higher values of $f_{\text{res}} = 52$ kHz for $s = 0$ and $f_{\text{res}} = 53$ kHz for $s = 100$, as seen in Fig. 7.2. Henceforth, it shall be implicit, that whenever we show plots for a certain value of s , it also implies the associated frequency of resonance.

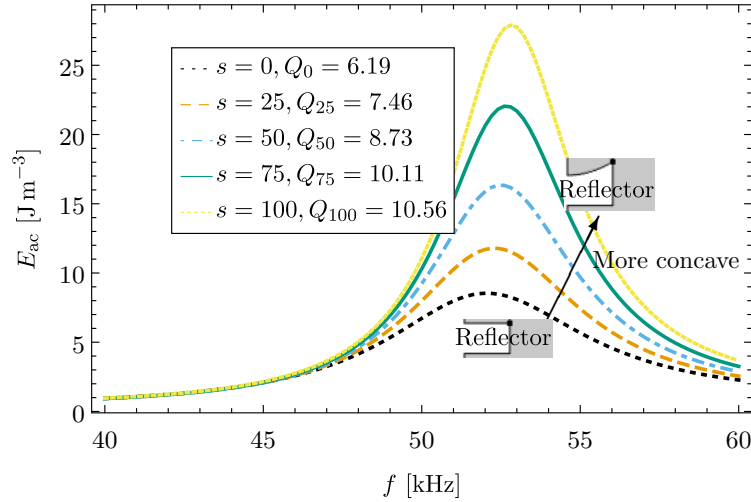


Figure 7.2: Energy density E_{ac} for five different values of s . As the reflector becomes more concave, more energy is held inside the domain of the levitator making it more powerful.

Clearly, the levitator contains more energy per volume for more concave reflectors. Additionally, the quality factor defined in Eq. (4.19), gets larger by a factor 1.71 from $s = 0$ to $s = 100$.

The conclusion is that, just as described by Xie and Wei [15], the acoustic waves are amplified and more concentrated around the axis of symmetry, when using the concave reflector, as seen in Fig. 7.3.

The acoustic pressure field p_1 has been solved for numerically by Comsol. The velocity field \mathbf{v}_1 was hereafter calculated through Eq. (4.7), and the acoustic radiation force per particle radius cubed, $\mathbf{F}_{\text{sa}}^{\text{rad}}/a^3$, was lastly calculated assuming the small particle limit $\delta \ll a \ll \lambda$, through the general expression Eq. (5.12a). When comparing Fig. 7.3(e) & (f) with Fig. 6.3(a), a resemblance of a sine wave is seen close to the axis of symmetry. Also, Fig. 7.3(a) & (b) is similar to a cosine pressure wave and Fig. 7.3(c) & (d) close to a sine velocity wave with twice the frequency as the pressure- and velocity waves. For the flat reflector, the resemblance is weakest, and for the concave reflector it is strongest. Note how (c) and (d) implies, that the resonance is not completely dominating, and that the off-resonant component of the velocity field is not neglectable. This is illustrated in Fig. 7.4.

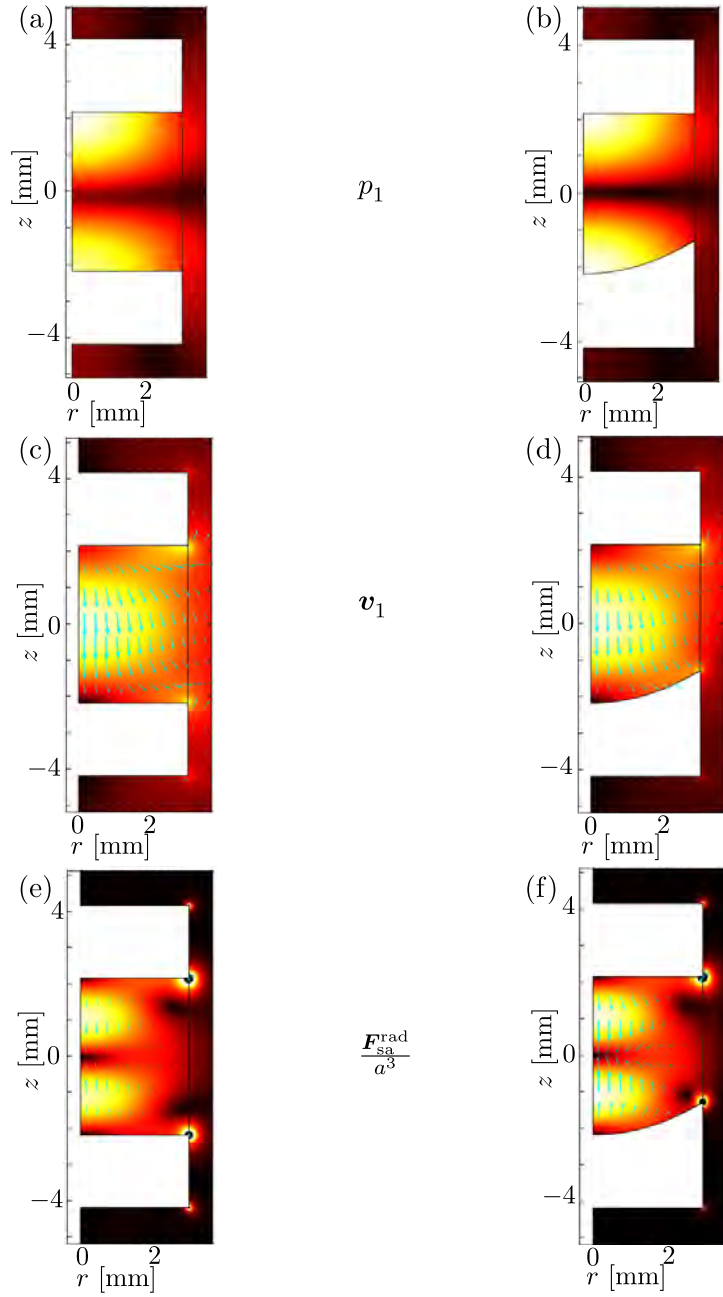


Figure 7.3: 4 The three acoustic fields plotted as absolute magnitude density plots, underneath a vectorplot of p_1 in (a) & (b), v_1 in (c) & (d) and $\mathbf{F}_{sa}^{\text{rad}}/a^3$ in (e) & (f). The reflector in (a), (c) and (e) are modelled for $s = 0$ and for $s = 100$ in (b), (d) and (f). The magnitude ranges for each plot as, (a) 0 Pa (black) to 3×10^3 Pa (white), (b) 0 Pa (black) to 5.5×10^3 Pa (white), (c) 0 m s^{-1} (black) to 7.5 m s^{-1} (white), (d) 0 m s^{-1} (black) to 14 m s^{-1} (white), (e) 0 N m^{-3} (black) to $1.2 \times 10^5 \text{ N m}^{-3}$ (white), and (f) 0 N m^{-3} (black) to $4 \times 10^5 \text{ N m}^{-3}$ (white).

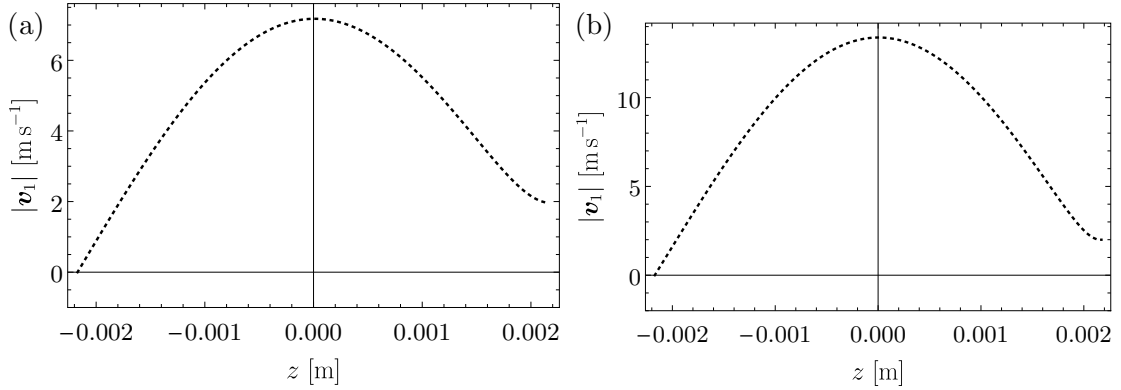


Figure 7.4: The absolute value of the velocity field $|\mathbf{v}_1|$ vs z , ranging from reflector to actuator, at $r = 0$ for (a) $s = 0$ and (b) $s = 100$. If we hit a “clean” resonance, as described in Section 4.2, the small off-resonant component, which equals the vibrating wall’s velocity on the vibrating wall would be insignificant compared to the resonant component.

Regarding the stability of the single-axis levitator, both Fig. 7.3(c) & (d) show a radial component of the radiation force. In order to determine stability of levitation we first calculate the difference between $(\mathbf{F}_{\text{sa}}^{\text{rad}})_z$ and the force of gravity \mathbf{F}_g at $r = 0$, to find possible levitation positions - see Fig. 7.5(a) and (c). Only the point where $\partial_z(\mathbf{F}_{\text{sa}}^{\text{rad}})_z < 0$ can be taken into consideration. Hereafter we inspect the radial component of $(\mathbf{F}_{\text{sa}}^{\text{rad}})_r$ along r at the possible levitation positions $z = z_{\text{lev}}$. Since both Fig. 7.5(b) and (d) show negative component, i.e. the radiation force is directed towards the centerline, the levitator is concluded to be stable in the two points $z_{\text{lev}} = -870.7 \mu\text{m}$ for $s = 0$ and $z_{\text{lev}} = -158.6 \mu\text{m}$ for $s = 100$.

The reader should further note that at each of the corners we encounter oddities, i.e. extremely strong fields (which are cropped on the density scale). They seem to be numerical singularities, as they vary highly with fineness of the constructed mesh. However, regardless of the fineness of the corner mesh, they do not disappear. By rounding off corners, their effect greatly decreases, yet do not disappear. Similarly by calculating the applied energy, dissipative energy and radiated energy into the PML, we found a discrepancy. Energy amounting to approximately 11.5% of the applied energy was unaccounted for. By considering the fact, that we only solve for the pressure field, and subsequently calculate the velocity field and radiation force, through gradients, any abrupt changes in the pressure field would result in huge velocity fields and forces. Thus, we must conclude that the physical model is not truly adequate.

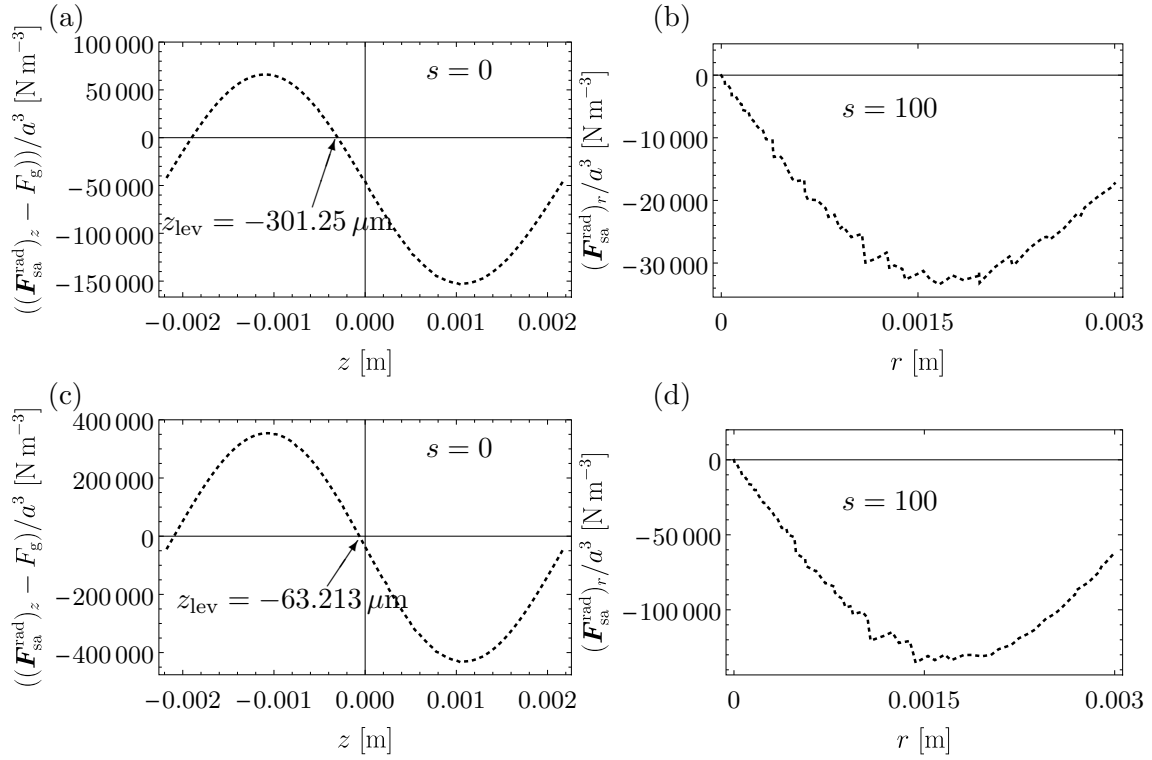


Figure 7.5: (a) The difference between z component of the small argument radiation force and the force of gravity per particle radius cubed. The arrow mark the possible stable position (z_{lev}) of levitation. (b) The radial component of the $\mathbf{F}_{sa}^{\text{rad}}$ calculated at $z = z_{\text{lev}}$. Similarly for (c) and (d). For (a) & (b) $s = 0$ and for (c) & (d) $s = 100$.

Chapter 8

Conclusion and outlook

In this thesis, the field of acoustic levitation has been studied, with the aim to determine stable levitation positions for particles. The results may have theoretical as well as practical applications. Thus, the results are applicable, where full control of stable levitation is crucial. This could be relevant in microgravitational experiments or in material processing.

To determine stable levitation with no restriction to the size relative to wavelength, an extension to the current theory describing the radiation force is called for. By applying first- and second-order perturbation theory and assuming $a \gg \delta, \delta_t$, we can ignore viscous and thermoviscous effects entirely. We thereby solve the inviscid Helmholtz wave equation for an ideal single-axis levitator. We conclude, that the actuated acoustic waves results in standing waves at resonance. Subsequently, we expand the exponential components of the standing wave. When a particle perturbs a levitator system, scattered waves written as an expansion in terms of scattering coefficients A_n , emerge. From these expansions we are able to derive an exact analytical expression, expressed as an infinite sum, for the acoustic radiation force. By assuming a water droplet suspended in air, we analyze the exact radiation force graphically as a function of the dimensionless wavenumber $x = 2\pi a/\lambda$. We find that including modes up to $N = 2$, results in Settnes and Bruus expression [10] in the small particle limit $a \ll \lambda$. Additionally, we conclude that for $a \gtrsim \lambda$ the acoustic radiation force makes a transition, and no longer scales as radius cubed. Hence, the radiation force becomes smaller relative to Settnes and Bruus expression. By the same token, including higher modes become of significant importance, in order to account for the full radiation force. Consequently, the stable particle levitation positions picks up a size dependency, whereas Settnes and Bruus expression does not. We conclude that, at first the stable positions shift towards the anti-nodes. Interestingly, we also conclude that for certain critical values of x , the acoustic force completely changes direction. These changes of direction are found to be related to force oscillations, and hence stable position oscillations, with respect to x .

In order to address the topic of actuating acoustic waves in a more realistic single-axis levitator, a Comsol model is created. Again assuming a water droplet suspended in air. By simulating the levitator, and testing the effect of concave reflectors, we conclude that the more concave reflector indeed strenghten the levitator in agreement with Xie's

and Wei's [15] experimental work. Additionally, we find the levitator to generate stable positions of levitation, when calculating the radiation force found by Settnes and Bruus. Consequently, the model may serve as an inspiration to future experimental single-axis levitators.

Outlook

Exact acoustic radiation force

Regarding the development of the exact expression for the radiation force, more time devoted to simplifying and reducing it, would have been desirable. Further analytical analysis of the dimensionless wavenumber limit, would make the graphical conclusions stronger, especially the small radius and wavelength ratio limit. Additionally, a thorough analysis of why we see acoustic radiation force oscillations with respect to x , was next to be made.

Finally, further extending the expression of the exact radiation force to in general include any kind of plane wave, would make the expression more applicable. The total radiation force of any wave written as a superposition of plane waves, would then be a sum of each associated radiation force.

The Comsol model

The Comsol simulation is the most time-consuming obstacle. Hence, the corner singularities are still to be thoroughly analysed. It is clearly a physical model issue, as they are highly dependent on fineness of mesh, as well as slightly rounding off corners. The first step would be to apply a better physical model, which would imply implementing a manually generated weak form PDE. Thus, the pressure field, as well as the velocity field, will be solved for. This leaves only the radiation force to be calculated. The purpose is to reduce the number of times, we would have to take derivatives, from twice to once, and so only enhance any abrupt changes once.

Finally, implementing the exact radiation force in the Comsol simulation, would be the ideal closure to this project.

Include other fluids and particles

When analyzing the exact radiation force and making simulations in Comsol, the next step would be to investigate, how the radiation force depend on the parameter ratios $\tilde{\rho}$ and $\tilde{\kappa}$. This would allow expanding the conclusions to include fluids and particles other than air and water.

Appendix A

Appendix to Chapter 3

A.1 Implementing PML

The theory behind PML will be briefly outlined in this section and only in one direction in cartesian coordinates. The theory is purely mathematical, and is a well known trick based on extending the coordinate system by a complex function. Hence, the propagating wave is damped, and if the function is well constructed, the wave will be reduced to zero before hitting any boundaries in a numerical calculation. As an example, assume a wave is propagating in the y -direction. We then introduce new coordinates \tilde{y} such that,

$$\partial_y = \frac{1}{1 + if(y)} \partial_{\tilde{y}}, \quad \text{with,} \quad f(y) = A \frac{(y_0 - y)^2}{L_{\text{PML}}}, \quad (\text{A.1})$$

where y_0 is the position at which the PML begins, and L_{PML} is the length of the PML. A is a parameter, which is adjusted to get the desirable dampening effect. The form of Eq. (A.1) is not necessarily a general one.

Consequently, whenever we perform any weak form PDE in a PML in Comsol, proper substitution must be carried out, e.g. rewriting the volumetric part of Eq. (3.7),

$$\int_{\Omega} \left[-\tilde{\nabla} \hat{g}_m(\mathbf{r}) \cdot \mathbf{J} - \hat{g}_m(\mathbf{r}) F \right] d\tilde{V} = \int_{\Omega} \left[- \left(\partial_x \mathbf{e}_x + \frac{1}{1 + if(y)} \partial_y \mathbf{e}_y + \partial_z \mathbf{e}_z \right) \hat{g}_m(\mathbf{r}) \cdot \mathbf{J} - \hat{g}_m(\mathbf{r}) F \right] (1 + if(y)) dx dy dz. \quad (\text{A.2})$$

This is the essential concept of PML, and applying PML for one-directional propagating waves is straightforward. However, when creating PML for arbitrary multi-propagating waves, the task becomes quite comprehensive, at least in order to get satisfying results. Fig. A.1 shows an attempt to self-create PML for a two-dimensional single-axis levitator, where all governing equations are implemented using the weak form PDE formulation described in Chapter 3. The conclusion is that the quality of the PML is not nearly good enough, as the propagating waves are not killed sufficiently fast. However, it does illustrate the concept.

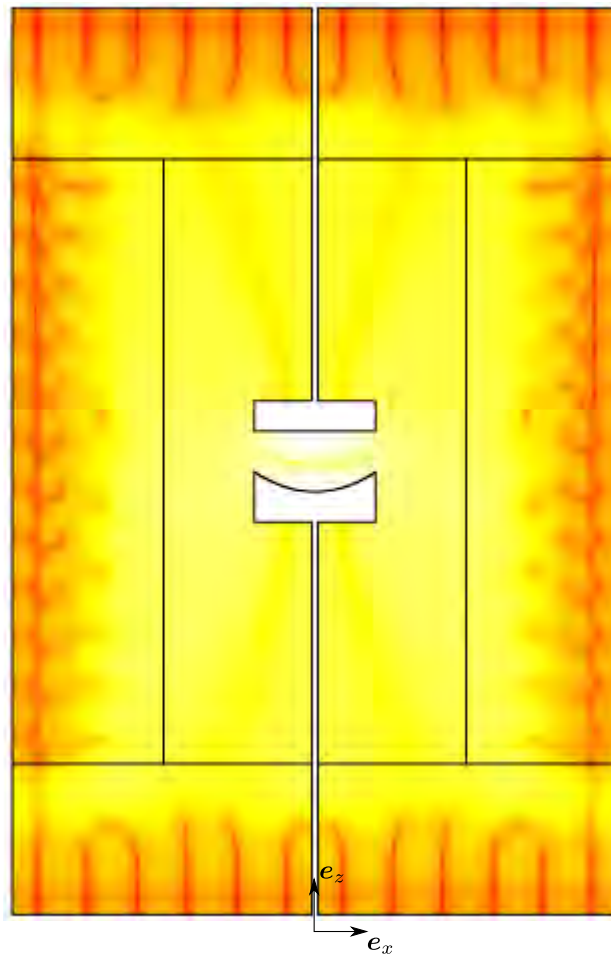


Figure A.1: A logarithmic plot of the acoustic pressure field. The outer squares are PML domain. Clearly, the PML does not attenuate the acoustic waves properly.

Appendix B

Appendix to Chapter 4

B.1 The general representation of the velocity field and thermoviscous and viscous boundary layers

This section serves to be a more elaborated section of the section with the same name in the main thesis.

Eqs. (4.7) and (4.8) gave the relation between \mathbf{v}_1 and ϕ_1 through Eq. (4.3), by neglecting the viscosity, or assuming a rotation free velocity field. However, without imposing such restrictions, a relationship between the velocity field and potential fields can still be found. The expressions and treatment thereof simply become more complicated. One has to be especially careful when operating with the Laplacian. Evidently both a scalar potential, ϕ and a vector potential $\boldsymbol{\psi}$ are used to fully express the velocity field, which shows through the Helmholtz decomposition.

According to the Helmholtz decomposition, the velocity field can in general be decomposed into the gradient of a scalar potential ϕ and the rotation of a divergence free vector potential $\boldsymbol{\psi}$,

$$\mathbf{v}_1 = \nabla\phi + \nabla \times \boldsymbol{\psi}, \quad \text{with} \quad \nabla \cdot (\nabla \times \boldsymbol{\psi}) = 0, \quad \nabla \times \nabla\phi = \mathbf{0}. \quad (\text{B.1})$$

In general the complete expressions of the Laplacian Eq. (2.3c) and Eq. (4.9) need to be taking into consideration in order to find solutions to an acoustofluidic system. To do this, the Navier–Stokes equation Eq. (4.3b) is divided into a compressional component containing $\nabla\phi_1$ and p_1 , and a rotational component containing $\nabla \times \boldsymbol{\psi}$.

The form of the scalar potential ϕ and vector potential $\boldsymbol{\psi}$ are determined by accounting for thermoviscous and viscous effects with the corresponding boundary conditions. These boundary conditions arise, whenever a fluid with applied acoustic fields, interacts with a another medium described by abrupt changes in physical parameters, such as compressibility and density. Examples would be a suspended particle or rigid walls parallel to acoustic wave propagation. Medium changes such as these, impose restrictions on the primary fluid at the boundary between fluid and e.g. particle or rigid wall. This effect is what give rise to viscous and thermoviscous boundary layers. The length of these boundary layers are giving by Ref [11],

$$\delta = \sqrt{\frac{2\nu_0}{\omega}}, \quad \delta_t = \sqrt{\frac{2D_t}{\omega}}, \quad \text{with} \quad \nu_0 = \frac{\eta_0}{\rho_0}, \quad D_t = \frac{k_t}{\rho_0 c_p}, \quad (\text{B.2})$$

where ν_0 is the momentum diffusion constant and D_t is the thermal diffusion constant given by the thermal conductivity k_t and specific heat capacity c_p .

Whenever we analyze a system a distance r away from a boundary with boundary layers, we use the term ‘‘bulk’’ when we are a distance $r \geq 5\delta, 5\delta_t$, to indicate that the boundary layers effect become neglectable.

The complete treatment of the acoustic fields that accounts for thermoviscous and viscous effects, has been made by Karlsen and Bruus [11] to determine the radiation force as mentioned in Chapter 1.

Since in Section 4.2, we will analytically investigate a single-axis levitator system in which we suspend a particle of radius $a \gg \delta, \delta_t$, and where no rigid walls which are parallel to wave propagation are present, we completely neglect viscous and thermoviscous effect in this thesis. We can consequently let $\nabla \times \boldsymbol{\psi} = \mathbf{0}$, and so the velocity rotation component drops out, leaving us with treating the acoustic fields in a special case for the remainder of this thesis, namely

$$\mathbf{v}_1 = \nabla \phi_1. \quad (\text{B.3})$$

B.2 Complete treatment of the solution to the ideal levitator setup

This section solves for the acutated fields in the ideal single-axis levitator as illustrated in Fig. 4.1.

The absence of any boundary walls parallel to the direction of wave propagation, ensures that the thermoviscous and viscous boundary layers never arises. The system is additionally consistent with that described by Eq. (4.8), and so the velocity potential, ϕ_1 must satisfy Eq. (4.6), for which the solution in one dimension can be written as two opposite propagating plane waves, with $k = k_0(1 + i\Gamma)$ and $k_0 = \omega/c_0$,

$$\phi_1(z, t) = \left(\phi_+ e^{ik_0 z} + \phi_- e^{-ik_0 z} \right) e^{-i\omega t}, \quad (\text{B.4})$$

where ϕ_+ and ϕ_- are two unknown complex constants to be determined by the boundary conditions. The velocity field is then,

$$\mathbf{v}_1(z, t) = ik \left(\phi_+ e^{ik_0 z} - \phi_- e^{-ik_0 z} \right) e^{-i\omega t} \mathbf{e}_z. \quad (\text{B.5})$$

The boundary conditions in Eq. (4.11) leads to $\phi_+ = \phi_-$ where,

$$\phi_+ = \phi_- = \frac{-\omega l}{2k \sin(kL)}, \quad (\text{B.6})$$

from which it follows that,

$$\mathbf{v}_1(z, t) = \frac{-\omega l}{\sin(kL)} \sin(kz) e^{-i\omega t} \mathbf{e}_z. \quad (\text{B.7})$$

By making a Taylor expansion of the velocity field in kL and kz around k_0L and k_0z and using $k_0\Gamma L \ll 1$ and $k_0\Gamma z \ll 1$, we find,

$$\mathbf{v}_1(z, t) \approx -\omega l \left(\frac{\sin(k_0z) + ik_0\Gamma z \cos(k_0z)}{\sin(k_0L) + ik_0\Gamma L \cos(k_0L)} \right) e^{-i\omega t} \mathbf{e}_z. \quad (\text{B.8})$$

Evidently, the radiation force turns out to be proportional to the amplitude squared of the velocity field and pressure field, and so it is highly desirable to maximize the amplitude of the standing waves in relation to the single-axis levitator. Maximum amplitude of Eq. (B.8) is achieved at resonance, when we are at minima in the denominator,

$$k_0 = k_n = n \frac{\pi}{L} = \frac{\omega}{c_0}, \quad \text{with } n = 1, 2, 3, \dots \quad (\text{B.9})$$

We thus define the n th angular frequency at resonance,

$$\omega_n = n \frac{\pi c_0}{L}. \quad (\text{B.10})$$

It should be stressed that the resonant angular frequencies ω_n in Eq. (B.10) are not exact, but exceptionally good approximations, as $k_0\Gamma L \ll 1$. At n th resonance we finally arrive at the following two acoustic fields for the levitator system,

$$\phi_1(z, t) \approx (-1)^n c_0 l \left(\frac{i}{n\pi\Gamma} \cos\left(n\pi \frac{z}{L}\right) + \frac{z}{L} \sin\left(n\pi \frac{z}{L}\right) \right) e^{-i\omega_n t}, \quad (\text{B.11a})$$

$$\mathbf{v}_1(z, t) \approx (-1)^n \omega_n l \left(\frac{-i}{n\pi\Gamma} \sin\left(n\pi \frac{z}{L}\right) + \frac{z}{L} \cos\left(n\pi \frac{z}{L}\right) \right) e^{-i\omega_n t} \mathbf{e}_z, \quad (\text{B.11b})$$

from which $p_1(z, t)$ and $\rho_1(z, t)$ can be calculated by Eq. (4.8) and Eq. (4.1).

B.3 Ignoring non-resonant component

Clearly, the resonant component of Eq. (B.11) satisfies the hard wall condition, i.e. $|\mathbf{v}_1(0, t)| = 0$ and $|\mathbf{v}_1(L, t)| = 0$, and is thus an eigenmode of the system. Thus, a single-axis levitator system which is actuated near resonant frequencies, excites the systems corresponding eigenmode, regardless of the actual boundary condition.

Eq. (B.11) further shows that the amplitude of the resonant component is far bigger than the non-resonant component, suggesting we might completely ignore it. The magnitude divided by $\omega_n l$ of the resonant component A_{res} and non-resonant component A_{nonres} of the velocity field are,

$$A_{\text{res}}(z) = \frac{\sin\left(n\pi \frac{z}{L}\right)}{n\pi\Gamma}, \quad (\text{B.12a})$$

$$A_{\text{nonres}}(z) = \frac{z \cos\left(n\pi \frac{z}{L}\right)}{L}, \quad (\text{B.12b})$$

where L has dimensions $[L] = \text{m}$.

Taking the derivative of each reveals that,

$$\partial_z A_{\text{res}}(z) = \frac{\cos\left(n\pi\frac{z}{L}\right)}{L\Gamma}, \quad (\text{B.13a})$$

$$\partial_z A_{\text{nonres}}(z) = -z\frac{n\pi\sin\left(n\pi\frac{z}{L}\right)}{L^2} + \frac{\cos\left(n\pi\frac{z}{L}\right)}{L}. \quad (\text{B.13b})$$

At the two walls, $z = 0$ or $z = L$, we find that $\partial_z A_{\text{res}}(z) \gg \partial_z A_{\text{nonres}}(z)$, assuming $\Gamma \ll 1$. Conclusively, just around the two walls, the resonant component will grow rapidly away from the walls. This implies, that the nonresonant part will have no effect on the velocity field around the stationary wall, $z = 0$. It further implies that the nonresonant component dominates extremely close to the vibrating wall. The distance from the vibrating wall, at which the absolute value of the resonant component is ten times bigger than the absolute value of the non-resonant part, $A_{\text{res}}(z) = 10A_{\text{nonres}}(z)$, is given by,

$$\frac{|n\pi\Gamma z \cos(n\pi z/L)|}{|L \sin(n\pi z/L)|} = \frac{|n\pi\Gamma z \cot(n\pi z/L)|}{L} = \frac{1}{10}, \quad \text{where } z < L. \quad (\text{B.14})$$

This reduces to

$$|z \cot(n\pi z/L)| = \frac{L}{n\pi\Gamma 10}. \quad (\text{B.15})$$

Utilizing that $\sin(\theta) \approx \pi - \theta$ and $\cos(\theta) \approx -1$ for $\theta \approx \pi$, we find $\cot(\pi z/L) \approx \frac{-1}{\pi - \frac{\pi z}{L}}$, and we get that,

$$|z \cot(n\pi z/L)| \approx \frac{z}{\pi - \frac{\pi z}{L}} = \frac{1}{\frac{\pi}{z} - \frac{\pi}{L}} = \frac{L}{n\pi\Gamma 10}. \quad (\text{B.16})$$

Which reduces to

$$z = \left(\frac{1}{L} + 10Ln\pi\Gamma\right)^{-1} \approx L(1 - 10n\pi\Gamma L^2), \quad \text{where } 10n\pi\Gamma L^2 \ll 1. \quad (\text{B.17})$$

Suppose $L \leq 10^{-2}$, $\Gamma \leq 10^{-4}$ and $n = 1$, the distance from the vibrating wall where the non-resonant component becomes insignificant, is at a distance $d = L - z_{\text{res}} \leq \pi 10^{-7}$. For all practical purposes, any particle or droplet of interest in this thesis, suspended in a single-axis levitator system, will be placed a distance greater than d from the vibrating wall, or it will have a radius a greater than d . Thus, it is unable to fit within the domain where the non-resonant component dominates. Regarding the scalar potential ϕ_1 and so also the pressure field, we see from Eq. (B.11a) that the non-resonant component dominates at $z = L/2$. By Eq. (4.7), we can readily estimate the relation between the resonant amplitude of the velocity field v_{res} and the non-resonant amplitude of the pressure field p_{nonres} at $z = L/2$,

$$\frac{p_{\text{nonres}}}{v_{\text{res}}} = \frac{\rho_0 c_0 \Gamma}{2}. \quad (\text{B.18})$$

In Chapter 5 we will see that the acoustic radiation force is determined by $\kappa_0 p_0^2$ and $\rho_0 v_0^2$, where $\kappa_0 = \frac{1}{\rho_0 c_0^2}$, p_a and v_a are the adiabatic compressibility, pressure amplitude and

velocity amplitude respectively. Using these scaled amplitudes, we arrive at the following ratio, using Eq. (B.18)

$$\frac{\kappa_0^{\frac{1}{2}} p_{\text{nonres}}}{\rho_0^{\frac{1}{2}} v_{\text{res}}} = \frac{\rho_0^{\frac{1}{2}} \kappa_0^{\frac{1}{2}} c_0 \Gamma}{2} = \frac{\Gamma}{2} \ll 1. \quad (\text{B.19})$$

Consequently we can in the ideal levitator system completely neglect the off-resonant components of the acoustic fields.

B.4 Acoustic energy density for harmonic waves

The acoustic energy density for an harmonically time oscillating system is twice the time-average of the kinetic energy density, which is given as

$$2 \langle E_{\text{kin}} \rangle = 2 \frac{1}{2} \frac{1}{L} \int_0^L dz \frac{1}{2} \rho_0 |v_1(z)|^2 = \frac{1}{L} \int_0^L dz \frac{1}{2} \rho_0 |v_1|^2, \quad (\text{B.20})$$

where the factor $\frac{1}{2}$ is from the time-average and the factor 2 is to account for twice the amount. By Eq. (B.7), we thus find, that close to resonance, where $k \simeq k_0 = n2\pi/\lambda = n\pi/L$,

$$E_{\text{ac}} = \frac{\rho_0 \omega^2 l^2}{4 |\sin(kL)|^2}. \quad (\text{B.21})$$

By performing a Taylor expansion in kL around resonance $k_0 L = k_n L = \frac{\omega_n}{c_0} L = n\pi$, where $k = (1 + i\Gamma) \frac{\omega}{c_0}$, we find that $\sin(kL) \approx \sin(k_0 L) + \cos(k_0 L)(kL - k_0 L) = \left(\frac{i\Gamma}{c_0} \omega + \frac{\omega - \omega_n}{c_0} \right) L$. Finally with $\omega \approx \omega_n$ we get,

$$E_{\text{kin}} = \frac{\rho_0 \omega^2 l^2}{4 \left| \frac{L}{c_0} (\omega - \omega_n) + i\Gamma n\pi \right|^2} = \frac{\rho_0 \omega^2 l^2}{4 n^2 \pi^2} \frac{\omega_n^2}{(\omega - \omega_n)^2 + \Gamma \omega_n^2}. \quad (\text{B.22})$$

Appendix C

Appendix to Chapter 5

C.1 Special functions

From Ref. [11] and citation therein, we will list the first two spherical Bessel- and spherical Hankel functions,

$$j_0(x) = \frac{\sin(x)}{x}, \quad j_1(x) = \frac{1}{x} \left(\frac{\sin(x)}{x} - \cos(x) \right), \quad (\text{C.1a})$$

$$h_0(x) = -i \frac{e^{ix}}{x}, \quad h_1(x) = -\frac{e^{ix}}{x} \left(1 + \frac{i}{x} \right). \quad (\text{C.1b})$$

For either a spherical Hankel or spherical Bessel function $g_n(x)$ the following recurrence relations apply, with prime denoting differentiation with respect to the argument,

$$\frac{d}{dx} [x^{-n} g_n(x)] = -x^{-n} g_{n+1}(x), \quad (\text{C.2a})$$

$$\frac{d}{dx} [x^{n+1} g_n(x)] = x^{n+1} g_{n-1}(x), \quad (\text{C.2b})$$

$$g'(x) = g_{n-1}(x) - \frac{(n+1)g_n(x)}{x}, \quad (\text{C.2c})$$

$$g'(x) = \frac{ng_n(x)}{x} - g_{n+1}(x), \quad (\text{C.2d})$$

$$g'(x) = \frac{1}{2} \left(g_{n-1}(x) - g_{n+1}(x) - \frac{g_n(x)}{x} \right). \quad (\text{C.2e})$$

For small arguments $x \ll 1$ and using Eq. (C.2c), we further find to leading order,

$$j_0(x) \simeq 1, \quad j'_0(x) \simeq -\frac{x}{3}, \quad (\text{C.3a})$$

$$j_1(x) \simeq \frac{x}{3}, \quad j'_1(x) \simeq \frac{1}{3}, \quad (\text{C.3b})$$

$$h_0(x) \simeq -\frac{i}{x}, \quad h'_0(x) \simeq \frac{i}{x^2}, \quad (\text{C.3c})$$

$$h_1(x) \simeq -\frac{i}{x^2}, \quad h'_1(x) \simeq 2\frac{i}{x^3}. \quad (\text{C.3d})$$

C.2 Deriving Eq. (5.19)

When deriving the small limit expression for the scattering coefficients, the starting point will be Eq. (5.18)

$$A_n = -\frac{j_n(x)}{h_n(x)} \left\{ \frac{1 - \tilde{\rho}\tilde{c} \frac{j_n(\frac{x}{\tilde{c}})j'_n(x)}{j_n(x)j'_n(\frac{x}{\tilde{c}})}}{1 - \tilde{\rho}\tilde{c} \frac{j_n(\frac{x}{\tilde{c}})h'_n(x)}{h_n(x)j'_n(\frac{x}{\tilde{c}})}} \right\}. \quad (\text{C.4})$$

Assuming $x \ll 1$ and $\frac{x}{\tilde{c}} \ll 1$ and using Appendix C.1, we find for A_0 to leading order that

$$A_0 \approx -\frac{1}{-\frac{i}{3x^3}} \left\{ \frac{1 - \tilde{\rho}\tilde{c}^2}{\tilde{\rho}\tilde{c}^2} \right\}, \quad (\text{C.5a})$$

$$= -\frac{ix^3}{3} \{1 - \tilde{\kappa}\}, \quad \text{where } \tilde{\kappa} = \frac{1}{\tilde{\rho}\tilde{c}^2}. \quad (\text{C.5b})$$

Similarly for A_1 we find to leading order

$$A_1 \approx -\frac{x}{-3\frac{i}{x^2}} \left\{ \frac{1 - \tilde{\rho}}{1 + 2\tilde{\rho}} \right\}, \quad (\text{C.6a})$$

$$= -\frac{ix^3}{3} \left\{ \frac{1 - \tilde{\rho}}{1 + 2\tilde{\rho}} \right\}, \quad (\text{C.6b})$$

$$= \frac{ix^3}{6} \left\{ \frac{2(\tilde{\rho} - 1)}{2\tilde{\rho} + 1} \right\} \quad (\text{C.6c})$$

Appendix D

Appendix to Chapter 6

D.1 Integration of tripple Legendre and Gegenbauer polynomials

This section serves to elaborate on the results giving in Section 6.1.

First we differentiate the Legendre polynomials in order to find

$$\partial_\theta P_n(\cos(\theta)) = -\sin(\theta)\partial_x P_n(x) = -\sin(\theta)C_{n-1}^{3/2}(x), \quad x = \cos(\theta) \quad (\text{D.1})$$

where C_n^λ are the Gegenbauer polynomials. By further substitution we arrive at

$$\partial_\theta P_n(\cos(\theta)) = -\sqrt{1-x^2}C_{n-1}^{3/2}(x), \quad x = \cos(\theta). \quad (\text{D.2})$$

Further we find that

$$\int_0^\pi d\theta f(\cos(\theta)) \sin(\theta) = \int_{-1}^1 dx f(x), \quad x = \cos(\theta). \quad (\text{D.3})$$

Eqs. (D.2) and (D.3) are readily used on Eq. (6.7) in order to find three different cases of tripple Legendre or Gegenbauer integrals. From Eq. (6.7a) we find,

$$\int_0^\pi d\theta P_n(\cos(\theta))P_m(\cos(\theta)) \cos(\theta) \sin(\theta) = \int_{-1}^1 dx P_n(x)P_m(x)x, \quad (\text{D.4a})$$

from Eq. (6.7b) we find,

$$\int_0^\pi d\theta \partial_\theta P_n(\cos(\theta))\partial_\theta P_m(\cos(\theta)) \cos(\theta) \sin(\theta) = \int_{-1}^1 dx C_{n-1}^{3/2}(x)C_{m-1}^{3/2}(x)(1-x^2)x, \quad (\text{D.4b})$$

and finally we find from Eq. (6.7c)

$$-\int_0^\pi d\theta P_n(\cos(\theta))\partial_\theta P_m(\cos(\theta)) \sin(\theta)^2 = \int_{-1}^1 dx C_n^{1/2}(x)C_{m-1}^{3/2}(x)(1-x^2). \quad (\text{D.4c})$$

Noting that $P_1(x) = C_1^{1/2}(x) = x$ we find by identification and comparison with the results found by S. Ališauskas [26] and Y. Hagiwara [27] that

$$\int_{-1}^1 dx P_n(x) P_m(x) x = \begin{cases} \frac{2n}{(2n-1)(2n+1)}, & \text{for } m = n - 1 \\ \frac{2(n+1)}{(2n+1)(2n+3)}, & \text{for } m = n + 1 \\ 0, & \text{otherwise,} \end{cases} \quad (\text{D.5})$$

and

$$\begin{aligned} - \int_0^\pi d\theta P_n(\cos(\theta)) \partial_\theta P_m(\cos(\theta)) \sin(\theta)^2 &= \int_0^\pi d\theta C_n^{1/2}(\cos(\theta)) C_{m-1}^{3/2}(\cos(\theta)) \sin(\theta)^3 \\ &= \frac{\pi(-1)^{(n-m+1)/2} (m+1)! \Gamma(J-1/2)}{4(m-1)! (J-m)! (J-n)! \Gamma(1/2) \Gamma(3/2) \Gamma(J+3/2)}, \end{aligned} \quad (\text{D.6a})$$

where $J = \frac{1}{2}(m+n+1)$, $\Gamma(\cdot)$ the gammafunction and $(\cdot)!$ the factorial function. When noting that the factorial function only takes integers greater than or equal to 0, we find $m \geq 1$.

Lastly we rewrite Eq. (D.4b) to find that

$$\begin{aligned} \int_0^\pi d\theta C_{n-1}^{3/2}(\cos(\theta)) C_{m-1}^{3/2}(\cos(\theta)) C_1^{1/2}(\cos(\theta)) \sin(\theta)^3 & \\ = \frac{\pi \Gamma(J' - n + 1/2) \Gamma(J' - m + 1/2) \Gamma(J' - 1/2)}{4 \Gamma(1/2) \Gamma(3/2) \Gamma(J' + 3/2)} & \end{aligned} \quad (\text{D.7a})$$

$$\times \sum_u \frac{(-1)^u (J' + 1 - u) [\Gamma(1/2 + u) \Gamma(3/2 - u)]^{-1}}{u! (1-u)! (J' - n - u)! (J' - m - u)! (J' - 2 + u)!}, \quad (\text{D.7b})$$

where we find the factorial and gamma function as before, and $J' = \frac{1}{2}(n+m+1)$. By noting the same restrictions apply to Eq. (D.7) as in Eq. (D.6), we find that

$$J' - n - u \geq 0 \Leftrightarrow m + 1 \geq n + 2u, \quad (\text{D.8})$$

and similarly

$$J' - m - u \geq 0 \Leftrightarrow n + 1 \geq m + 2u. \quad (\text{D.9})$$

Combining Eqs. (D.8) and (D.9) we get

$$-2u + n + 1 \geq m \geq n + 2u - 1, \quad -2u + m + 1 \geq n \geq m + 2u - 1. \quad (\text{D.10})$$

This is only possible if $u = 0$, and if so, $(J' - 2 + u)!$ makes the following restrictions $m + n \geq 3$.

S. Ališauskas further impose the following restrictions to the tripple Gegenbauer integrals,

$$\frac{1}{2}(m+n-1) \in \mathbb{N}, \quad \text{or} \quad \frac{1}{2}(m+1-n) \in \mathbb{N}, \quad \text{or} \quad \frac{1}{2}(n+1-m) \in \mathbb{N}. \quad (\text{D.11})$$

Thus, implying that $m = n \pm 1$, when accounting for the previous-mentioned restrictions.

D.2 Derivation of Eq. (6.20)

By the definition of the compressibility Eq. (4.2) we find that the maximum change in volume to first order in the derivative, is

$$\kappa_p = -\frac{1}{V} \frac{\partial V}{\partial p} \simeq \frac{1}{a^3} \frac{(a + a_1)^3 - a^3}{p + p_1 - p} \simeq \frac{3a_1}{ap_1}, \quad (\text{D.12})$$

where we assumed $a_1 \ll a$. Isolating the ratio of interest, we find,

$$\frac{a_1}{a} \simeq \frac{\kappa_p}{3} p_1 = \frac{\kappa_p c_0^2 \rho_0 \rho_1}{3\rho_0} = \frac{\tilde{\kappa}}{3} \epsilon_{ac}. \quad (\text{D.13})$$

Appendix E

Appendix to Chapter 7

E.1 Solving Helmholtz wave equation in cylindrical coordinates

The inviscid Helmholtz wave equation Eq. (4.16) will in this section be solved in cylindrical coordinates for the pressure field, in a single-axis levitator setup. We can express the wave equation as follows

$$\nabla^2 p_1 = \frac{1}{r} \partial_r (r \partial_r p_1) + \frac{1}{r^2} \partial_\theta^2 p_1 + \partial_z^2 p_1 = -k^2 p_1. \quad (\text{E.1})$$

By separation of variables, we express the pressure field as $p_1 = R(r)\Theta(\theta)Z(z)$ and by interting this into Eq. (E.1) we get,

$$\frac{1}{r}(R'\Theta Z) + R''\Theta Z + \frac{1}{r^2}\Theta''ZR + Z''\Theta R = -k^2 p_1, \quad (\text{E.2})$$

where prime denotes differentiation with respect to the argument, and the arguments have been suppressed. By deviding through with p_1 , we find

$$\frac{R'}{rR} + \frac{R''}{R} + \frac{\Theta''}{r^2\Theta} + \frac{Z''}{Z} = -k^2. \quad (\text{E.3})$$

For Eq. (E.3) to hold for all r , θ and z we find that

$$\frac{R'}{rR} + \frac{R''}{R} + \frac{\Theta''}{r^2\Theta} + k^2 = -\frac{Z''}{Z} = l^2, \quad (\text{E.4})$$

where $l \in \mathbb{C}$. Solving Eq. (E.4), we find $Z(z) = ae^{ilz} + be^{-ilz}$, where $\{a, b\} \in \mathbb{C}$. In a levitator setup, such as the one build in Comsol in Chapter 7, we assume that if we hit resonance, the resonant component will dominate, and a cosine pressure wave will be actuated (as of Section 4.2), in which case the boundary condition yields

$$\partial_z p_1 = 0, \quad \text{for } z = \{0, L\}. \quad (\text{E.5})$$

Thus, we find $l = m\frac{\pi}{L}$, with $m \in \mathbb{N}$ and $Z(z) = Z_0 \cos(lz)$, where Z_0 is an amplitude.

Having found l we then write,

$$\frac{R'}{rR} + \frac{R''}{R} + k^2 - l^2 = \frac{\Theta''}{r^2\Theta} = n^2, \quad n \in \mathbb{C}. \quad (\text{E.6})$$

Just as with the z dependency the solution comes out as $\Theta(\theta) = \alpha e^{in\theta} + \beta e^{-in\theta}$, where $\{\alpha, \beta\} \in \mathbb{C}$. The boundary condition in the azimuthal symmetric case yields

$$\Theta(\theta) = \Theta(\theta + 2\pi), \quad \partial_\theta \Theta(\theta) = \partial_\theta \Theta(\theta)|_{\theta=\theta+2\pi}, \quad \forall \theta. \quad (\text{E.7})$$

By utilizing the orthogonality of $e^{in\theta}$ and $e^{-in\theta}$, we find $n \in \mathbb{N}$, and hence $\Theta(\theta) = \Theta_0 e^{\pm in}$, where Θ_0 is an amplitude, and $e^{\pm in\theta}$ implies superposition.

Lastly, we end up with,

$$r^2 R'' + rR' + [r^2(k^2 - l^2) - n^2] R = 0. \quad (\text{E.8})$$

The general solution to Eq. (E.8), which must be defined at $r = 0$, is the Bessel function [29], which are expressed as follows,

$$R(r) = R_0 J_m(\varrho r), \quad (\text{E.9})$$

where $\varrho^2 = k^2 - l^2$ and R_0 is some amplitude.

Finally, the solution to the pressure field is found to be,

$$p_1(r, \theta, z) = p_A J_n(\varrho r) e^{\pm in\theta} \cos\left(zm \frac{\pi}{L}\right), \quad (\text{E.10})$$

where p_A is some wave amplitude, $m \in \mathbb{N}$, and ϱ is determined by appropriate boundary conditions.

E.2 Parameters used in Comsol

A listing of the, in Comsol, used parameters loaded as a .txt file. The left side lists parameter name, and the right lists their value.

```
H 0.5*cAIR/fH
fH 40[kHz]
R 3[mm]
cAIR 347.4[m/s]
etaAIR 18.54e-6[Pa*s]
rhoAIR 1.161[kg/m^3]
kapAIR 1/(rhoAIR*cAIR^2)
f0 40[kHz]
omg 2*pi*f0
d0 6[um]
vol pi*R^2*H-1/2*con*pi*R^4 volume
Gamma 0.005*0+beta*etaAIR*omg/(2*rhoAIR*cAIR^2)
fpre cAIR/R/(2*pi)
```

```
k0 omg/cAIR
vbc omg*d0
Rrod 0.5[mm]
Rbox 8[mm]
Hbox 19[mm]
Hact 2[mm]
Href 2[mm]
lam cAIR/fH
lamH lam/2
Hpml Hbox+2*Dpml
Rpml Rbox+Dpml
Dpml 0.8*lam
con 100[m-1] Size of concave reflector
beta 0.9266
kapWA 4.451e-10[Pa-1]
rhoWA 996.6[kg*m-3]
fco0 1-(kapAIR/kapWA)-1
fco1 2*(rhoWA/rhoAIR-1)/(2*rhoWA/rhoAIR+1)
curvr 2*100[um]*0
viscwall sqrt(2*(etaAIR/rhoAIR)/omg)
stvol Rbox*Hbox-(R*(H+2*Href))
boxl 0.001/2*0
g 9.82[m*s-2]
Fg 4/3*pi*rhoWA*g
zbal -63.213[um]
```


Bibliography

- [1] H. Bruus, J. Dual, J. Hawkes, M. Hill, T. Laurell, J. Nilsson, S. Radel, S. Sadhal, and M. Wiklund, *Forthcoming lab on a chip tutorial series on acoustofluidics: Acoustofluidics-exploiting ultrasonic standing wave forces and acoustic streaming in microfluidic systems for cell and particle manipulation*. *Lab Chip* **11**(21), 3579–3580 (2011).
- [2] P. Augustsson, C. Magnusson, M. Nordin, H. Lilja, and T. Laurell, *Microfluidic, label-free enrichment of prostate cancer cells in blood based on acoustophoresis*. *Anal. Chem.* **84**(18), 7954–7962 (2012).
- [3] F. Petersson, A. Nilsson, C. Holm, H. Jönsson, and T. Laurell, *Separation of lipids from blood utilizing ultrasonic standing waves in microfluidic channels*. *Analyst* **129**(10), 938–43 (2004).
- [4] L. V. King, *On the acoustic radiation pressure on spheres*. *Proc. R. Soc. London, Ser. A* **147**(861), 212–240 (1934).
- [5] K. Yosioka and Y. Kawasima, *Acoustic radiation pressure on a compressible sphere*. *Acustica* **5**, 167–173 (1955).
- [6] L. P. Gorkov, *On the forces acting on a small p in an acoustical field in an ideal fluid*. *Sov. Phys.–Dokl.* **6**(9), 773–775 (1962), [*Doklady Akademii Nauk SSSR* **140**, 88 (1961)].
- [7] A. A. Doinikov, *Acoustic radiation force on a spherical p in a viscous heat-conducting fluid .1. general formula*. *J. Acoust. Soc. Am.* **101**(2), 713–721 (1997).
- [8] A. A. Doinikov, *Acoustic radiation force on a spherical p in a viscous heat-conducting fluid .2. force on a rigid sphere*. *J. Acoust. Soc. Am.* **101**(2), 722–730 (1997).
- [9] A. A. Doinikov, *Acoustic radiation force on a spherical p in a viscous heat-conducting fluid .3. Force on a liquid drop*. *J. Acoust. Soc. Am.* **101**(2), 731–740 (1997).
- [10] M. Settnes and H. Bruus, *Forces acting on a small particle in an acoustical field in a viscous fluid*. *Phys. Rev. E* **85**, 016327 (2012).
- [11] J. T. Karlsen and H. Bruus, *Forces acting on a small particle in an acoustical field in a thermoviscous fluid*. *Phys. Rev. E* **92**, 043010 (2015).

- [12] H. Bruus, *Acoustofluidics 7: The acoustic radiation force on small particles*. Lab Chip **12**, 1014–1021 (2012).
- [13] A. L. YARIN, M. PFAFFENLEHNER, and C. TROPEA, *On the acoustic levitation of droplets*. Journal of Fluid Mechanics **356**, 65–91 (1998).
- [14] F. B. Wijayal and K. M. Lim, *Numerical calculation of acoustic radiation force and torque on non-spherical particles in Bessel beams*, chap. 139, 2071 (Acoustical Society of America) (2016), abstract for the 171st Meeting Acoustical Society of America.
- [15] W. Xie and B. Wei, *Parametric study of single-axis acoustic levitation*. Appl. Phys. Lett. **79**(6), 881–883 (2001).
- [16] E. H. Brandt, *Acoustic physics. Suspended by sound*. Nature **413**(6855), 474–5 (2001).
- [17] V. Vandaele, P. Lambert, and A. Delchambre, *Non-contact handling in microassembly: Acoustical levitation*. Precis. Eng. **29**(4), 491–505 (2005).
- [18] H. Bruus, *Acoustic streaming notes* (2015), unpublished lecture notes.
- [19] E. B. Tadmor, R. E. Miller, and R. S. Elliott, *Continuum mechanics and thermodynamics : from fundamental concepts to governing equations*, chap. Introduction, 1–2 (Cambridge University Press) (2012).
- [20] H. Bruus, *Theoretical Microfluidics* (Oxford University Press, Oxford) (2008).
- [21] C. P. Nielsen, *Introduction to weak form modeling in comsol* (2013), a Comsol guide developed for the Theoretical Microfluidics Group at the Department of Physics at the Technical University of Denmark.
- [22] H. Bruus, *Implementation of first- and second-order acoustic perturbation theory in comsol* (2016), comsol notes.
- [23] P. B. Muller and H. Bruus, *Numerical study of thermoviscous effects in ultrasound-induced acoustic streaming in microchannels*. Phys. Rev. E **90**(4), 043016 (2014).
- [24] H. Cohl and C. MacKenzie, *”Generalizations and specializations of generating functions for jacobi, gegenbauer, chebyshev and legendre polynomials with definite integrals”*. ArXiv e-prints (2012).
- [25] R. Szmytkowski, *Some differentiation formulas for Legendre polynomials*. ArXiv e-prints (2009).
- [26] S. Alisauskas, *Coupling coefficients of $SO(n)$ and integrals involving jacobi and gegenbauer polynomials*. Journal of Physics A: Mathematical and General **35**(34), 7323 (2002).
- [27] Y. HAGIWARA, *Applications of gaunt’s integral to some problems in physical geodesy*. Journal of Physics of the Earth **23**(4), 311–321 (1975).

- [28] T. Hasegawa and K. Yosioka, *Acoustic radiation force on a solid elastic sphere*. J. Acoust. Soc. Am. **46**, 1139–1143 (1969).
- [29] M. R. Spiegel, S. Lipschutz, and J. Liu, *Mathematical Handbook of Formulas and Tables*, chap. Five (McGraw Hill), 4th edn. (2013).